Improving the description of the suspended particulate matter concentrations in the southern North Sea through assimilating remotely sensed data

El Serafy, G.Y.; Eleveld, M.A.; Blaas, M.; van Kessel, T.; Gaytan Aguilar, S.; van der Woerd, H.J.

published in
Ocean Science Journal
2011

DOI (link to publisher)
10.1007/s12601-011-0015-x

document version
Publisher's PDF, also known as Version of record

Ocean Sci. J. (2011) 46(3):179-204
http://dx.doi.org/10.1007/s12601-011-0015-x

Article

Available online at www.springerlink.com

SpringerLink

Ocean Science Journal

Improving the Description of the Suspended Particulate Matter Concentrations in the Southern North Sea through Assimilating Remotely Sensed Data

Ghada Y. El Serafy[1,2]*, Marieke A. Eleveld[3], Meinte Blaas[1], Thijs van Kessel[1], Sandra Gaytan Aguilar[1], and Hendrik J. Van der Woerd[3]

[1]*Marine and Coastal Systems, Deltares, Rotterdamseweg 185, PO Box 177, 2600 MH Delft, Netherlands*
[2]*Delft University of Technology, Delft Institute of Applied Mathematics, Mekelweg 4, 2628 CD, Delft, Netherlands*
[3]*Vrije Universiteit Amsterdam, Institute for Environmental Studies (VU-IVM), De Boelelaan 1087, 1081 HV Amsterdam, Netherlands*

Received 14 June 2011; Revised 17 September 2011; Accepted 24 September 2011

Abstract – The integration of remote sensing data of suspended particulate matter (SPM) into numerical models is useful to improve the understanding of the temporal and spatial behaviour of SPM in dynamic shelf seas. In this paper a generic method based on the Ensemble Kalman Filtering (EnKF) for assimilating remote sensing SPM data into a transport model is presented. The EnKF technique is used to assimilate SPM data of the North Sea retrieved from the MERIS sensor, into the computational water quality and sediment transport model, Delft3D-WAQ. The satellite data were processed with the HYDROPT algorithm that provides SPM concentrations and error information per pixel, which enables their use in data assimilation. The uncertainty of the transport model, expressed in the system noise covariance matrix, was quantified by means of a Monte Carlo approach. From a case study covering the first half of 2003, it is demonstrated that the MERIS observations and transport model application are sufficiently robust for a successful generic assimilation. The assimilation results provide a consistent description of the spatial-temporal variability of SPM in the southern North Sea and show a clear decrease of the model bias with respect to independent in-situ observations. This study also identifies some shortcomings in the assimilated results, such as over prediction of surface SPM concentrations in regions experiencing periods of rapid stratification/de-stratification. Overall this feasibility study leads to a range of suggestions for improving and enhancing the model, the observations and the assimilation scheme.

Key words – data assimilation, sediment transport, remote sensing, Kalman filter, North Sea

*Corresponding author. E-mail: ghada.elserafy@deltares.nl

1. Introduction

Suspended particulate matter (SPM) is composed of fine-grained inorganic particles and material of organic origin that is suspended in the water column. SPM plays an important role in the ecology of shelf seas such as the southern North Sea. SPM influences the underwater light climate, which is an important environmental factor for phytoplankton growth (McQuatters-Gollop et al. 2007). Moreover, the organic fraction of SPM can be an important source of nutrients (Van Beusekom et al. 1999; Weston et al. 2008; Vermaat et al. 2008). Finally, the transport and fate of SPM influences the fate of adsorbed micro-pollutants and trace metals (Laane et al. 1999; Stronkhorst et al. 2003; Klamer et al. 2005).

The North Sea sediment transport system is characterized by highly variable concentrations in time and space: re-suspension events during high wave conditions, formation of eddies and meanders, variable river inflow and tidal currents all contribute to the complexity of the system (Simpson and Souza 1995; Eleveld et al. 2008; Pietrzak et al. in press, Dobrynin et al. 2010). Modelling such a system has its difficulties and accuracy limitations.

Traditionally, observations of SPM have relied on regular ship-based sampling, occasionally extended to dedicated field campaigns. Nowadays, automated *in situ* monitoring buoys enable the recording of continuous time series of SPM at in increasing number of sites for prolonged periods

of time (e.g. Kröger et al. 2009). Moreover, with the arrival of reliable ocean colour remote sensing data (e.g. CZCS, SeaWiFS, and more recently, NASA's MODIS sensors and ESA's MERIS sensor) more frequent synoptic mapping of sea surface SPM has become feasible with increasing spatial resolution. Subsequently, new algorithms for coastal shelf seas have been developed (e.g. Doerffer and Schiller 2007 and Van der Woerd and Pasterkamp 2008). Finally, merging of global ocean data is currently being performed with techniques that produce uniform data products together with measurable uncertainty bounds for chlorophyll concentration, combined dissolved and detritus absorption coefficient, and SPM backscattering coefficient (Maritorena et al. 2010). These developments enable a new level of describing and understanding the physical and biological dynamics in coastal seas including SPM transport (Robinson et al. 2002).

However, all *in situ* and remote sensing techniques have their limitations when sampling such a heterogeneous system. *In situ* samples are mostly sparse in space and/or time, while the optical remote sensing only measures the surface layer whereas a large portion of the SPM is found near the bed. In these instances, three-dimensional, process-based modelling can provide complementary information about the coastal transport system (Baumert et al. 2000; Delhez et al. 2004). Recent examples of integration of remote sensing data and numerical models of the southern North Sea are the paper of De Boer et al. (2009) and Fettweis et al. (2007). De Boer et al. (2009) applied sea surface temperature (SST) imagery and a three-dimensional numerical model of a river plume to detect up welling induced by tidal straining in the Rhine region of fresh water influence (ROFI). Fettweis et al. (2007) carried out a study where satellite images (SeaWiFS), in situ measurements (tidal cycle and snapshot) and a 2D hydrodynamic numerical model have been combined to calculate the long term SPM (Suspended Particulate Matter) transport through the Dover Strait and in the southern North Sea.

However, also modelling suffers from limitations in accuracy due to the propagation of uncertainties in hydro-dynamic forcing on SPM behaviour, initial conditions and boundary conditions, in addition to uncertainties in the parameterization of processes such as water-bed exchange of sand-mud mixtures. The governing equations may contain inaccuracies due to lack of knowledge about the complex physical processes and their interactions. Also, resolution reduction and simplifications are often necessary to avoid high computation times, which add to the model's uncertainty. To contribute to the understanding of model uncertainties and improve model predictions, data assimilation techniques such as Kalman filter techniques can be applied. Those techniques combine model output with recent measurement data, using the information on the uncertainties in the model and the measurements to give a better estimate of the model forecast.

In recent years, various data-model integration efforts have been using new sources of observational information and formal statistical methods to further describe and understand the North Sea SPM transport model uncertainties. Gerritsen et al. (2000) and Vos et al. (2000) made a pioneer study on how remotely sensed reflectance images can provide additional information on the spatial distribution of (sea surface) suspended sediment using inverse and Goodness-of-Fit (GoF) approaches. Such approach is useful for structured sensitivity analysis providing a quantified assessment of the strengths and weaknesses of modelling and input data. Allen et al. (2007) summarise error statistics for a complex 3D model in the southern North Sea using a wealth of observational data. They demonstrate that to understand model data misfit and the mechanisms creating errors, is essential to assess the distribution of model errors spatially and temporally. They use a hierarchy of techniques, including simple correlations, model bias, model efficiency, binary discriminator analysis.

More sophisticated techniques such as Kalman filters are applied mainly for open ocean models of slowly varying parameters like sea-surface temperature and sea-surface height (Testut et al. 2003; Keppenne et al. 2005). In the coastal areas the number of studies with Kalman filters is still limited (Chen et al. 2009; Wei and Malanotte-Rizzoli 2009).

The Ensemble Kalman filter (EnKF) introduced by Evensen 2003 is a very generic data assimilation technique that is suitable for highly nonlinear models such as those describing the sediment transport. An EnKF-based data assimilation technique was used by Margvelashvili et al. 2008, to assimilate average mean SPM concentration to the three-dimensional fine-resolution numerical models of sediment transport applied to the Torres Strait region of northern Australia. Very recently, Stroud et al. 2010 used the EnKF and a smoothing algorithm to assimilate a sequence of SeaWiFS satellite images in Lake Michigan in

with a sediment transport model to produce maps of sediment concentrations and uncertainties over space and time. They address the high dimensionality, measurement bias, and nonlinearities inherent in satellite data.

In this paper, remotely sensed SPM concentrations are assimilated in a numerical transport model by means of a generic data assimilation technique, Ensemble Kalman Filtering (EnKF). The paper summarizes the application of the EnKF and discusses results of a case study. It explores to what extent the assimilated model can characterise the spatial and temporal description of SPM in the southern North Sea. The results of the study are also intended to foster model development and to improve the accuracy of the predictions and operational forecasts. The approach of the study is outlined in Figure 1, which indicates the processing of the remote sensing data, the model setup and the validation against in situ data. In this paper, we follow the same structure. First, we present the production and an analysis of the MERIS SPM products and their accuracy; thus indicating the opportunities they offer for data assimilation. Secondly, the numerical transport model system is described and the spatial and temporal nature of its solutions is discussed. Thirdly, the assimilation approach and description of the underlying assumption on the errors in both the model and the measurements are presented. Subsequently, the results of assimilating the remotely sensed SPM products in the transport model are compared first to the MERIS data as a verification step of the technical application of the assimilation experiment and then to the independent in situ field data from various sources to assess whether a better description of the system is obtained. Finally the paper is finalized by discussion conclusions and recommendations.

2. Remote Sensing Data Set

Remotely sensed SPM for the assimilation originates from the MEdium Resolution Imaging Spectrometer (MERIS) instrument on board ESA's ENVISAT spacecraft. For the year 2003, MERIS Reduced Resolution (nominally 1.2 km) atmospherically corrected (Level 2) reflectance data (ESA 2006) were processed with the HYDROPT

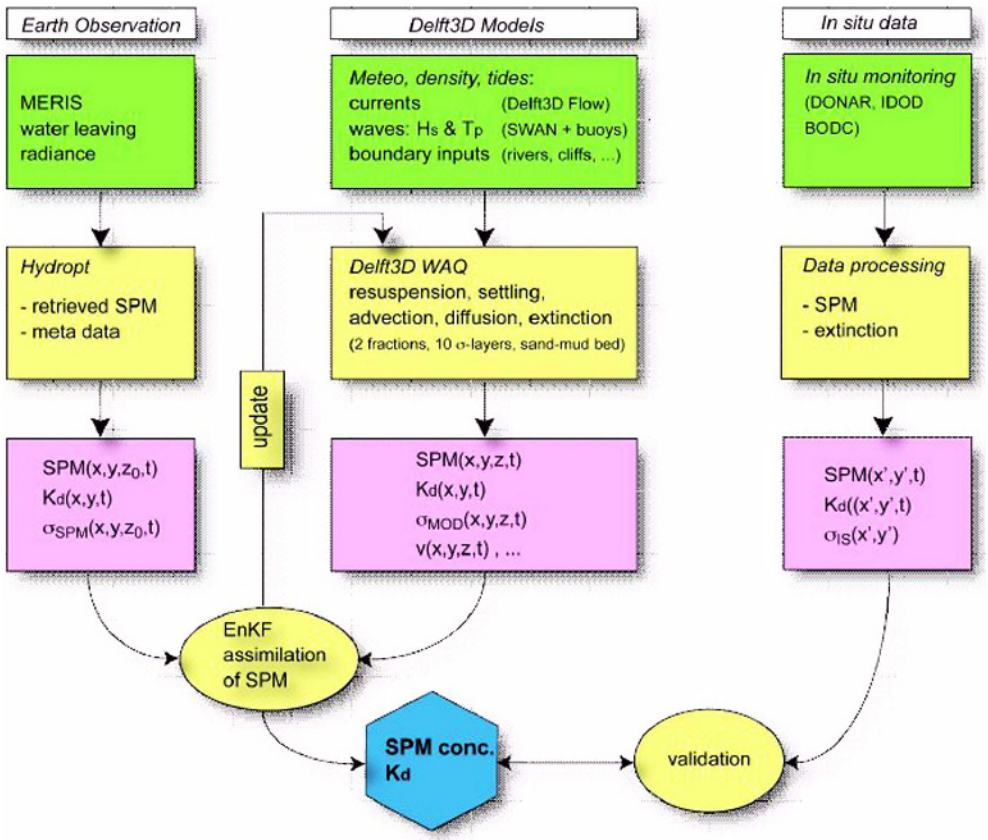

Fig. 1. Scheme of the data assimilation procedure presented to obtain improved data sets of SPM concentrations

algorithm (Van der Woerd and Pasterkamp 2008) to obtain SPM concentration data in the North Sea.

Retrieval method

HYDROPT comprises a forward model and an inverse model. The forward model generates a lookup table (LUT) of water-leaving radiance reflectance (ρ_w) as a function of among others the Inherent Optical Properties (IOPs) absorption (a) and scattering (b) of North Sea water and its constituents chlorophyll (CHL), SPM and coloured dissolved organic matter (CDOM). The forward model is based on the Hydro Light radiative transfer model (Mobley and Sundman 2001). The inversion is based on least-square fitting of the MERIS measured reflectances to the modelled reflectances (Doerffer and Fisher 1994; Garver and Siegel 1997; Maritorena et al. 2002). In this study, the inversion comprised χ^2 fitting of MERIS measured $\Delta\rho_w$ for consecutive bands to the modelled $\Delta\rho_w$ stored in the LUT (Mobley et al. 2005; Van der Woerd and Pasterkamp 2008). Bio-optical modelling with specific IOPs enables retrieval of the concentrations of CHL, SPM and CDOM from these reflectances. The HYDROPT inversion was run with a set the specific IOPs for CHL, SPM and CDOM (Table 1) that was optimised for the Belgian and Dutch coastal zone (Tilstone et al. submitted). The Ensemble Kalman filter technique requires that each SPM measurement also has an estimate of the standard error. Those standard errors vary per retrieved concentrations per pixel. The standard errors do not reflect a structural spatial dependence but they show high values around clouds. In HYDROPT confidence intervals (referred to as standard errors, σ) of the retrieved CHL, SPM and CDOM concentrations were determined from χ^2 intervals around the fitted values (Van der Woerd and Pasterkamp 2008; *cf.* Press et al. 1992 Chap 15 for details).

Regarding confidence in MERIS (ρ_w), note that the MERIS Level 2 Product Confidence Data flag for ρ_w (PCD_1_13) was applied (*cf.* ESA 2006). In addition, χ^2 fit values and probabilities were derived; the latter from the cumulative (Gamma) distribution function (cdf) $P(\chi^2|df)$. Moreover, the vertical diffuse attenuation coefficient (K_D) values at 560 nm were generated. The inverse of K_D serves as a first approximation of optical depth, $\varsigma=1/K_{D560}$ (m) (Gordon and McCluney 1975).

Then, the daily datasets with metadata were passed on to the Ensemble Kalman Filtering toolbox. These comprise HYDROPT SPM concentrations, their latitude-longitude grids, error products (χ^2, P and σ_{SPM}), and the vertical attenuation coefficients at 560 nm (K_{D560}). They also consist of ESA Level 2 metadata, such as timestamps and Product Coding flags, notably the PCD_1_13 flag for negative reflectance, glint, white caps and atmospheric correction (ESA 2006).

The quality of HYDROPT SPM data has been extensively checked against in situ SPM measurements and response to environmental factors such as tidal conditions (Peters et al. 2008; Van der Wal et al. 2010, respectively).

Quality control of near shore coastal products

Figure 2 shows the currently retrievable water quality parameters CHL, SPM and CDOM with their retrieval errors (σ) Figure 2 also indicates the depth of the top layer of the North Sea (optical depth) from which the concentrations of SPM and other optically active substances, such as CHL and CDOM have been retrieved. Comparing independent

Table 1. For wavelengths corresponding to the MERIS bands, the absorption and scattering (in m^{-1}) of pure seawater, the absorption per unit concentration for chlorophyll-*a* (m^2 mg^{-1}), absorption and scattering per unit concentration for suspended particular matter (m^2 g^{-1}), and absorption (m^{-1} normalized at 440 nm) of coloured dissolved organic matter. Scattering of CHL (and CDOM) were assumed zero

Wavelength	Absorption	CHL	SPM	CDOM	Scattering	SPM
	Pure seawater				Pure seawater	
413	0.007	0.0231	0.0499	1.0686	0.0072	0.4344
442	0.0106	0.0252	0.0378	0.9953	0.0053	0.4118
490	0.0181	0.0205	0.0243	0.8882	0.0034	0.3783
510	0.0326	0.0122	0.0202	0.8471	0.0029	0.3576
560	0.0669	0.0064	0.0127	0.7524	0.0019	0.3508
620	0.2805	0.0129	0.0073	0.6526	0.0012	0.3363
665	0.3992	0.0179	0.0048	0.5865	0.0009	0.3072
681[a]	0.4343	0.0095	0.0066	0.002	0.0008	0.2999

[a]Band 8 (wavelength 681) was not used because of a possible contribution of fluorescence to the reflectance signal

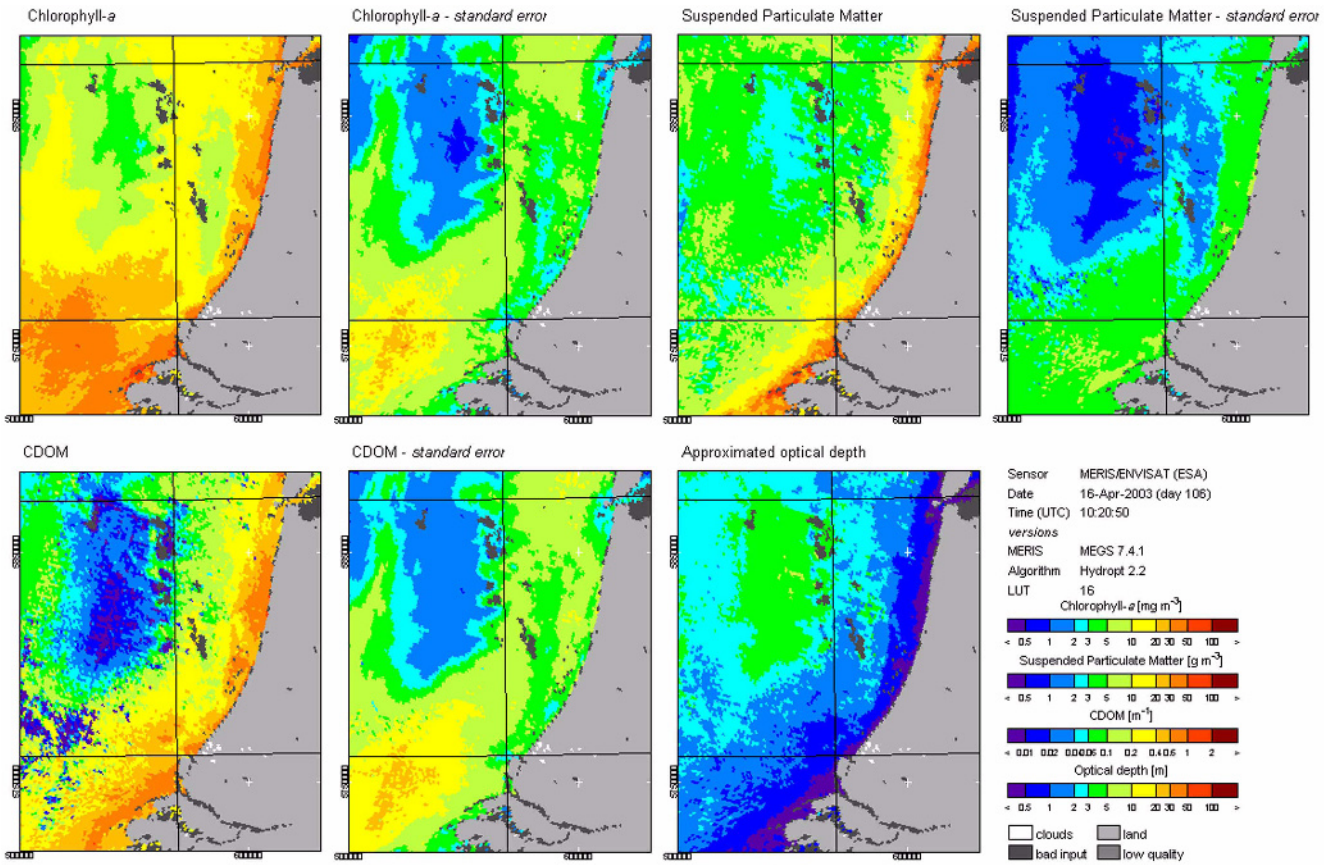

Fig. 2. Water quality parameters and error products. Near shore optical depth (approximated by 1/KD560) is limited

panels in Figure 2 shows that optical depth is low (< 1 m) near shore, where many optically active substances reside, and higher (3-5 m) near the offshore where the turbidity is minimum. Also, cross-shore gradient in bio-geophysical products (i.e. concentrations) is large.

The high near shore reflectance due to the large number of scatterers (high sediment load) might impact the atmospheric correction, and lead to saturation of the water reflectance signal in the shorter wavelength bands (Ruddick et al. 2000, 2007). However, a check on the quality of atmospheric properties, Level 2 reflectances, and the retrieved SPM concentrations along transect near Noordwijk (52.25 N, 4.43 E) shows that the data products that we pass on to the Ensemble Kalman Filtering toolbox can be used from 1 km offshore onwards. First, atmospheric properties remain stable along transect until 1 km from the first land-pixel (Figure 3a). Secondly, reflectance in the near-infrared (from about 780-1400 nm) is low over water until 1 km offshore, because of high water absorption at these wavelength, while reflectance at 560 nm - which is strongly dependent on SPM scattering and less dependent on CHL and CDOM absorption (Eleveld et al. 2008) - increases towards the turbid coastline (Figure 3b). Thirdly, the retrieval with HYDROPT gives realistic SPM results offshore and near shore, and the absolute errors remain within bounds near shore (Figure 3c).

3. SPM transport Model Description

The applied numerical model suite comprises the Delft3D Flow hydrodynamic model (Stelling and van Kester 1994; Lesser et al. 2004), the surface wave model SWAN (Booij et al. 1999) and the sediment transport and water quality model Delft3D-WAQ (e.g. Van Gils et al. 1993; Los et al. 2004; Postma and Hervouet 2008). These models are applied on a domain covering the southern North Sea (Figure 4). The horizontal grid spans 65 columns × 134 rows. Horizontal resolution is highest in the coastal areas of interest, notably the Dutch coastal zone (to ~ 2×2 km). The grid is coarser in the outer parts of the model domain (to ~

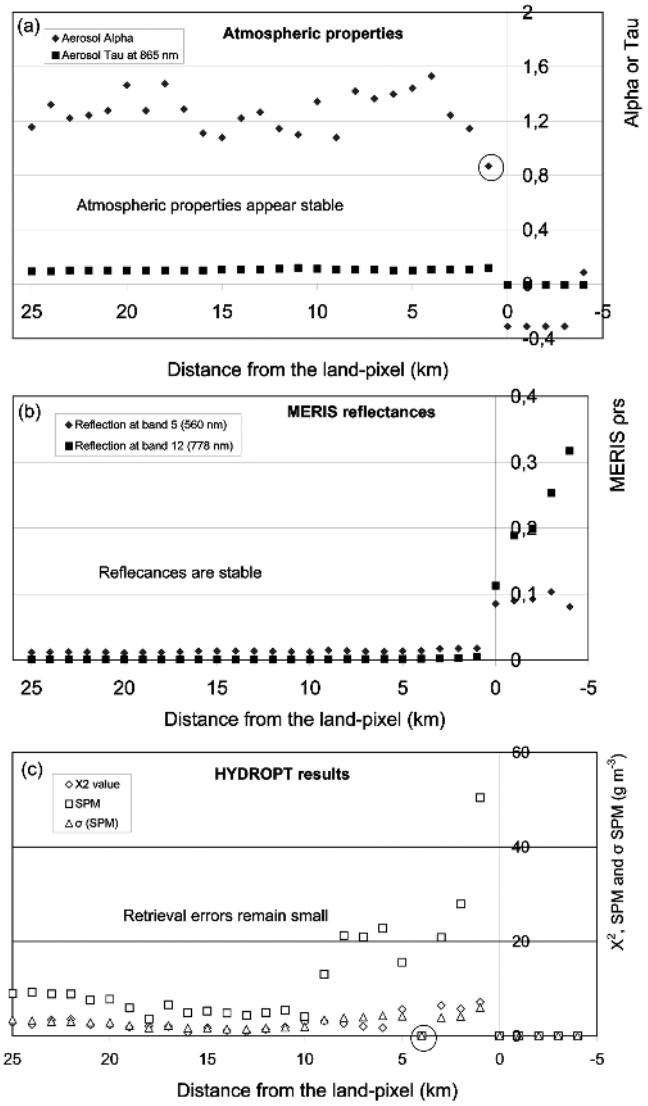

Fig. 3. (a) Atmospheric properties, (b) MERIS reflectances, and (c) The retrieved concentrations along a transect near Noordwijk (52.25 N, 4.43 E)

20×20 km). In the vertical 10 sigma-layers are applied. Near the bed and near the surface, the layer thickness is about 4 percent of the local water depth to enable good resolution of the surface mixing layer and the elevated near-bed SPM concentrations. At mid-depth, the layer thickness is approximately 20 percent of the local water depth.

The water motion is governed by tidal, wind and density effects. Astronomic tides have been prescribed at the open boundaries. Atmospheric forcing has been derived from hind casts of the Dutch met-office limited area atmospheric model (HIRLAM, KNMI, see also http://hirlam.org, http://www.knmi.nl/datacentrum). In addition, rivers discharges of fresh water have been prescribed as point sources adopted from national databases (http://live.waterbase.nl, http://www.ceh.ac.uk/data/nrfa/index.html, http://seine-aval.crihan.fr/web, www.nlwkn.niedersachsen.de, www.arge-elbe.de, www.bafg.de).

Resuspension due to surface waves, especially during strong wind events, is a key factor determining the SPM concentrations in the coastal seas. In order to obtain a model that describes the patterns of resuspension sufficiently accurate given the model resolution, significant wave height and mean wave period data are required as input to determine the wave-induced bottom shear stress (Soulsby 1997). To achieve the desired accuracy, a data-model integration technique has been applied in which wave buoy observations are combined with the SWAN wave model results. The temporal evolution of the wave parameters has been obtained from spectra measured at 6 wave buoys in the southern North Sea (shown in Figure 4) and the spatial interpolation is carried out with the aid of the spatial patterns in wave parameters derived from a SWAN wave model simulation for 2003.

The Delft3D-WAQ sediment transport model computes the advection-diffusion, settling and resuspension of SPM in two silt fractions given the transport velocities, mixing

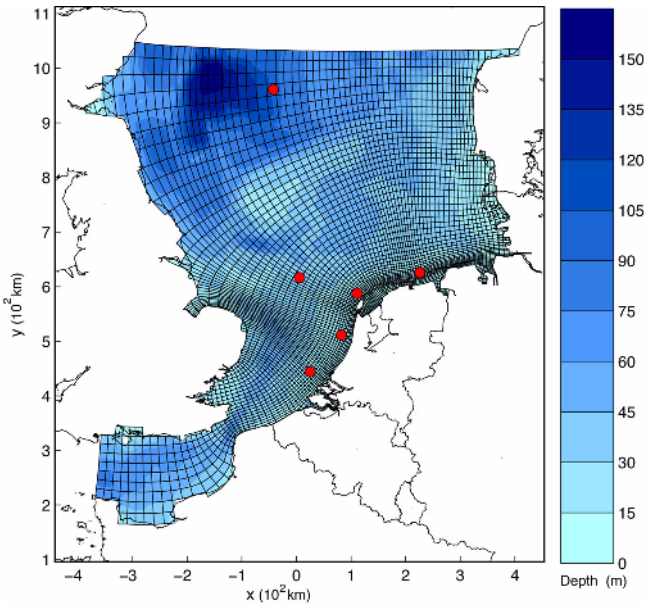

Fig. 4. Horizontal grid of the Southern North Sea model applications, together with the bathymetry. The wave buoy observation locations used in the wave model calibration are also shown as red dots. The individual hydrodynamic, wave and transport models all operate on this grid

coefficients and bed shear stresses adopted from the hydrodynamic and wave models. Recently, Delft3D-WAQ has been extended with an improved parameterisation of the resuspension and buffering of silt fractions from and in a predominantly sandy seabed (Van Kessel et al. 2010). This parameterisation enabled a realistic description of the periodic and relatively limited resuspension during the tidal cycle and the massive resuspension from deeper bed layers observed during high wave events. (See also the results below in Figure 16).

The transport model is provided with lateral boundary conditions based on climatological SPM concentrations, SPM loads from the rivers and specific point or line sources representing erosion of cliffs that feed turbid zones such as the East Anglian Plume and the Flemish Banks. The model solution for 2003 is part of a multi-annual model experiment using water motion and wave information from 1996 onward. During the preparation of this experiment, the solution, especially of the slowly responding bed composition, has been properly equilibrated. Van Kessel et al. 2010 discuss these results in more detail and demonstrate the model's ability to reproduce the low and high frequency components of the SPM signals.

It should be noted however, that most *in situ* data used in the model development consist of the relatively low-frequency monitoring data of the Dutch and Belgian authorities (Rijkswaterstaat 2008; MUMM 2008; see sampling sites in Figure 5). This may imply a reduced accuracy in the description of features such as the East Anglian plume off the UK coast. Also, it is known that the two incorporated size fractions are more representative for the southern of the North Sea than for the central North Sea (northern part of the domain) where the SPM has different characteristics and dynamics.

Figure 6 illustrates the typical nature of the input and responses of the various model components. It is beyond the scope of this paper to extensively discuss the hydrodynamic, wave and transport model results, but a few representative results confirm the general quality and will be helpful when interpreting the results of the SPM model in section [Assimilation Experiment Results].

The hydrodynamic and transport models are both supplied with time varying data that show events in river discharge (Figure 6, Panel (1) shows the daily running mean values of these). In particular in January, February and March relatively high discharges occur that last one to weeks. The fresh

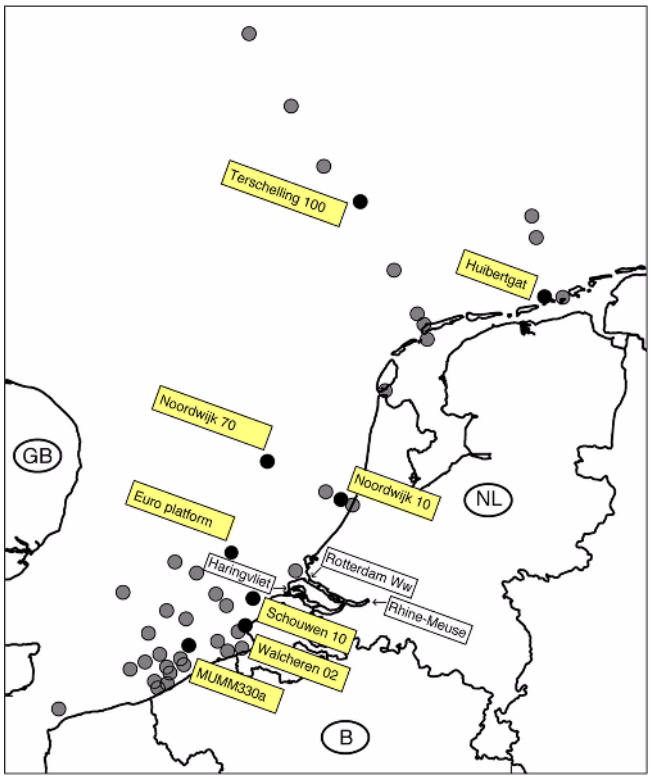

Fig. 5. Zoom of the model domain, indicating the measurement locations discussed in the text. All relevant in situ data sampling sites are indicated by a bullet: the the black bullets are explicitly discussed in section [Assimilation Experiment Results]. Also indicated are the discharge locations of the Rhine-Meuse rivers

water enters the North Sea at the sites indicated in Figure 4 and is transported and mixed by the prevailing currents. Due to earth rotation, the residual transport of the riverine waters is northward along the continental coast. Panel (2) in Figure 6 shows the time series of surface salinity at Noordwijk 10 km offshore, about 40 km north of the northern river mouth (Rotterdam Waterway) and another 15 to 20 km north of the southern river mouth (Haringvliet) (Figure 5). The modelled series shows a lagged response in decreased surface salinities. The first two discharge events are predominantly taking place through the sluices of the Haringvliet and the time lag is notably larger and amplitude relatively smaller than in the later events which are taking place through the Rotterdam waterway. The in situ data of surface salinity at Noordwijk 10 confirm the model results in terms of the low-frequency evolution, but also suggest the model is underestimating the salinity in this particular near-shore area. The third panel of Figure 6 shows the daily running mean of the wind speed at the Euro platform

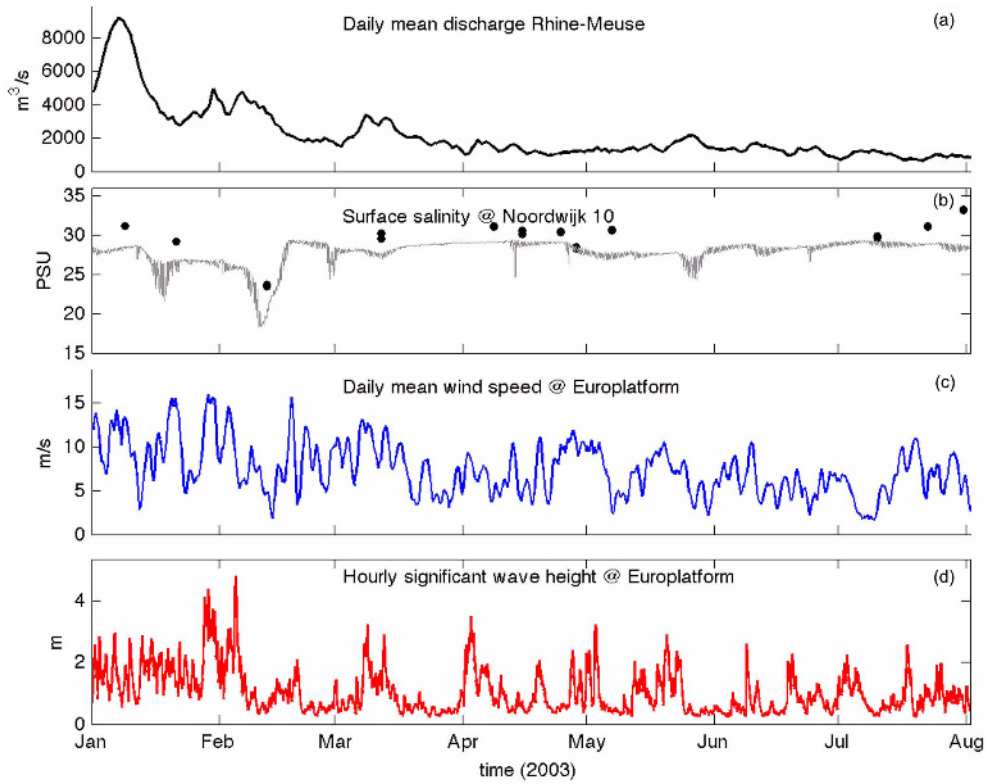

Fig. 6. Time series illustrating typical model input and model output fort he first seven months of 2003. Panel (a) daily average volume discharge of combined Rhine-Meuse river system, (b) Surface salinity at Noordwijk 10 km offshore (grey results Delft3D Flow model, black in situ measurement data (Rijkswaterstaat 2008), (c) Daily mean of imposed wind speed extracted from 22 km HIRLAM atmospheric model grid at location of Europlatform. (d) Significant wave height at Europlatform (wave buoy signal is virtually identical to blend of wave model and buoy at this site). Daily running means have been chosen for plotting clarity

measurement site, approximately 50 km offshore of the Rhine-Meuse river mouths. The data show the typical wind events with a frequency of about once to twice per week associated to the general weather patterns. The wind speed peak amplitudes decrease from 10 to 15 m/s in the winter months to just around 10 m/s at most in spring and summer. Wind directions are predominantly westerly (not shown). Panel (4) shows the response in terms of significant wave height at Euro platform. The mean wave periods are varying between about 4 to 6 s, indicating that the waves in the southern North Sea are mostly locally generated. The resulting modelled bottom shear stresses due to the combination of waves and currents vary more strongly spatially than the wave height and are shown along with the panels of the SPM concentrations below.

4. Data Assimilation Methodology

The sediment transport model as described in section [SPM transport Model Description] computes the advection-diffusion, settling and resuspension of SPM in two silt fractions given the transport velocities, mixing coefficients and bed shear stresses adopted from the hydrodynamic and wave models. This dynamical system of the suspended particulate matter, SPM, propagated in time k can be described as follows

$$c_{k|k-1} = f(c_{k-1|k-1}) \quad (1)$$

Where $c_{k|k-1}$ will be addressed as state/system space vector and is composed of the two silt fractions that composes the suspended particulate matter at time k at all layers of the model.

The Ensemble Kalman Filter (EnKF)

The procedure of the Ensemble Kalman Filter is designed as follows:

The sediment transport model propagates the system space state vector, SPM concentration in the water column, $c_{k|k-1}$, in time as in equation (1). At each time, t_k, an ensemble of size N is generated of the state vector. The

ensemble is generated with a mean $\hat{c}_{k|k-1}$ representing the initial condition (analysis) of the state vector and with a covariance matrix $P_{k|k-1}$ representing the uncertainty in the analysis conditioned on previous measurements up to and including time t_{k-1}. This error covariance matrix is describing the spatial correlation of the error in the silt fractions at the whole model grid at time t_{k-1}.

At every time step, t_k, each ensemble member, i, with its state vector, $c^i_{k|k-1}$, perturbed additively by model errors, w^i_k, is propagated in time through the dynamical model system as follows

$$c^i_{k|k-1} = f(c^i_{k-1|k-1}) + w^i_k \quad (2)$$

The model errors, w^i_k, are randomly drawn from a predefined distribution with zero mean and an error covariance matrix, Q_k. This error covariance matrix represents the structure of the uncertainties in the model. The assumptions on the error covariance matrix are discussed further in section [Error Covariance matrices structure]. These model errors can be regarded as the system noise.

The estimate of the update (forecast) of the state vector is calculated, at any time step, through the mean of the ensemble as

$$\hat{c}_{k|k-1} = \frac{1}{N}\sum_{i=1}^{i=N} c^i_{k|k-1} \quad (3)$$

The error covariance matrix in the estimate of the time update (forecast) of the state vector, $P_{k|k-1}$, is calculated as the error covariance matrix of the ensemble

$$P_{k|k-1} = L_{k|k-1}L'_{k|k-1}$$

$$\text{where } L_{k|k-1} = \frac{1}{\sqrt{N-1}}\sum_{i=1}^{N}(c^i_{k|k-1} - \hat{c}_{k-1}) \quad (4)$$

and $L'_{k|k-1}$ is the transpose of $L_{k|k-1}$.

Apart from the model state ensemble, random perturbations are added to the remote-sensing SPM concentration measurements to follow the assumption on the measurements as a stochastic variable. An ensemble of size N of possible observations, y^i_k, is generated on the actual observations, using measurement errors, v_k. The measurement errors are also randomly generated from a predefined distribution with zero mean and covariance matrix, R_k, representing the uncertainties in the measurements. Using the measurement operator H, the state vector is mapped to the measurement domain as further discussed in section [Spatial mapping between model and observations].

The Kalman gain can then be determined by

$$K_k = P_{k|k-1}H'_k(H_kP_{k|k-1}H'_k + R_k)^{-1} \quad (5)$$

The Kalman gain is seen as a weighting function between the model error and the measurement error.

Furthermore, the measurement updated state vector (analysis) for every ensemble is then calculated as

$$x^i_{k|k} = x^i_{k|k-1} + K_k(y^i_k - H_kx^i_{k|k-1}) \quad (6)$$

For the sake of understanding the physical significance of the Kalman gain, the scalar case of equation (5) is addressed by

$$K_k = \frac{\sigma^2_{c_{k|k-1}}}{(\sigma^2_{c_{k|k-1}} + \sigma^2_{y_k})} \quad (7)$$

For a large model errors compared to measurement errors ($\sigma^2_{c_{k|k-1}} >> \sigma^2_{y_k}$), the Kalman gain approaches 1 (i.e. a full weight is given to the satellite measurements and no weight is given to the model) and vice versa, the Kalman gain approaches 0 (i.e. the measurements are disregarded) and the update is the modelled SPM. For the non scalar case, each of the Kalman gain columns represents, loosely addressed, the spatially redistribution weight of the difference between the measurements and the model output.

Using the results of Equation (6), the estimate of the measurement update (corrected silt fractions of SPM) and the error covariance matrix are calculated as the mean of the ensemble, $\hat{c}_{k|k}$, and the covariance of the ensemble, $P_{k|k}$.

The updated state is then used in the dynamical system to get the forecast at time k+1 as follows in a sequential form

$$\hat{c}_{k+1|k} = f(c^i_{k|k}) \quad (8)$$

The full EnKF formulation is to be found in Evensen (2003). The advantage of the ensemble Kalman filter is the feasibility of fast generic implementation in complex and non-linear models.

Theoretically speaking the assimilation redistributes spatially the differences between the measurements and the model. If both measurements and model description are physically consistent, there is no matter being produced nor destroyed through the update.

Moreover, since the state contains silt fractions at all layers of the model and since the measurements are only of the surface layer, the translation to the vertical is carried out through the K as shown in equation (6), the Kalman gain as

mentioned is a weighting function that expresses also the vertical correlation calculated by the ensemble members that are propagated through the model and contain in theory all information from the model equations.

Re-starting the model upon correction with MERIS data implies a mismatch between the model solution and boundary conditions (at open boundaries, and the water-bed exchange). This mismatch may continue for quite some time, as amount of SPM and distribution do not match the boundary conditions of the model. A comparison of the open boundaries used in the model and the measurements to be used in the assimilation has been carried out. The comparison showed that there is no significant mismatch at the open boundaries. Due to that reason, it was not essential to deal explicitly with that issue since the boundaries are quite far enough from the area of interest and the insignificant mismatch is corrected for after the first time step of restarting the model. Since the model time step is 10 minutes and this updating procedure is at most every day due to image availability, there is enough time for the model to adjust for this very slight inconsistency (if any). In case of the water-bed exchange, the time scale of the water-bed exchange of matter is slower than the exchange rate in the water column across layers. This gives even more time for the bed to adjust to the changes in the water column through the model. However, this is a point to be considered in the follow up research as written in the recommendation.

In the current study an ensemble of 30 members is perturbed with the additive noise generated under the assumptions as discussed below. This size of the ensemble was deemed to be sufficiently large to statistically represent the error definitions and the filter statistics. While on the other hand, it did not cause too much of a computational burden that would hamper the experiment. Initial trial tests showed that an increase in the size of the ensemble would not result in significant differences in the results.

Error Covariance matrices structure

A key aspect in the application of data assimilation is the use of known or assumed uncertainties or errors in both measurements given by the measurement error covariance matrix, R_k, and errors in the model expressed in its covariance matrix, Q_k. In practice, the structures of those two matrices are not known and have to be assumed. The quality of these assumptions affects the performance of the filter.

Measurement uncertainties

The measurement error covariance matrix, R_k, includes measures of the accuracy of the instruments, the measuring technique and the retrieval method. For the MERIS-observed SPM concentration, the magnitude of the uncertainties in the measurements are given by the standard deviation of the retrieved data provided by HYDROPT, as explained in section [Remote Sensing data set]. Given the nature of the retrieved SPM concentrations it is difficult to know if, and if so to what degree the errors made on two different retrieved values are correlated. In practice, it is assumed that the errors in retrieved SPM concentrations are uncorrelated in space. The measurement error covariance matrix, R_k, is thus a diagonal matrix. Since the satellite observes only the upper surface of the ocean within the optical depth, it is assumed that the MERIS observed SPM is equivalent to the modelled SPM within the surface layer of the model (i.e. MERIS observes the upper layer of the model).

Model uncertainties

Defining the so-called system noise or model error (Q_k) is nontrivial in complex models. The system noise represents all influences not modelled or not considered during conceptualization of the model. Thus, the magnitude of the system noise covariance matrix (Q_k) is a measure of the model uncertainty. The better the model describes reality, the smaller the system noise. The structure of the uncertainties in the model and typical correlation scales that underlay the noise covariance matrix, however, is not straightforwardly known. Usually, assumptions on the model error are based on experience gained during the calibration and validation of the model. In practice, the performance of the filter will tell if the assumption on the error covariance matrix, Q_k, is adequate. For the water quality model Delft3D-WAQ, uncertainties are assigned only to the suspended particulate matter concentrations (i.e. independent variables in the filtering sense). The bed sediment concentrations were considered to be a "certain" source and/or sink. At present, all other variables such as hydrodynamic variables and wave variables are considered to be sufficiently accurate driving forces for the sediment transport model and are not part of the state vector. Compared to the uncertainty in modelling of the SPM concentration, the uncertainty in the hydrodynamic variables and the wave variables are relatively minor. They are based on offline calculations that have been separately calibrated as discussed in section [SPM transport

Model Description]. For future research, hydrodynamic and wave variables, such as bottom shear stress, vertical stratification, vertical mixing coefficient and transport velocities or their driving agents might be included provided that sufficient measurements are available.

In the EnKF, the system noise is assumed to follow a known Gaussian distribution characterised by its expectation value and its covariance matrix (Evensen 2003). Since the model is assumed not to underestimate or overestimate the state (i.e. no systematic spatial bias at each time step), the expected value of the system noise should be zero, E[w]=0. The variances of the errors are a measure of the accuracy of the model. The spatial correlations represent the correlation between errors at a given element of the matrix representing a grid cell to its spatial surrounding grid cells. In most situations, the correlation scales in the structure of the covariance matrix of the system noise, Q_k, are not known exactly. In practice, Q_k is specified based on physical reasoning and the correlation scale of the model errors. If the correlation scale is large, this indicates that the model error at a given grid cell is correlated to the error made at spatially remote cells as well. If the correlation scale is small, the error made at a grid cell is correlated to only very close and/or adjacent cells.

In this paper, a Monte Carlo approach (e.g. Evensen 1994) is also used to help define an estimate of the correlation structure in the covariance of the system noise. This idea is based on computing the noise evolution within the dynamical system (i.e. propagation of a prior assumption of the noise) through an ensemble and calculating the correlation length scales of the output error at every time interval in a given time window. The average of those correlation scales is regarded as an indication of the natural correlation scales of the system (El Serafy and Mynett 2008), given the noise distribution of the prior assumption. Here, an iterative procedure is applied to generate a physically consistent assumption of the correlation scales of the system noise covariance matrix Q_k. The procedure is sketched in Figure 7. Starting by selecting prior assumptions of the dominant correlation scale, λ, a covariance matrix is calculated and used to generate an ensemble run for successive periods of one month. The correlation scale is calculated at every given time interval in the one month period. The time average of the correlation scale is then calculated. If the average is bigger than the prior assumptions, the correlation scale is increased for the following iteration,

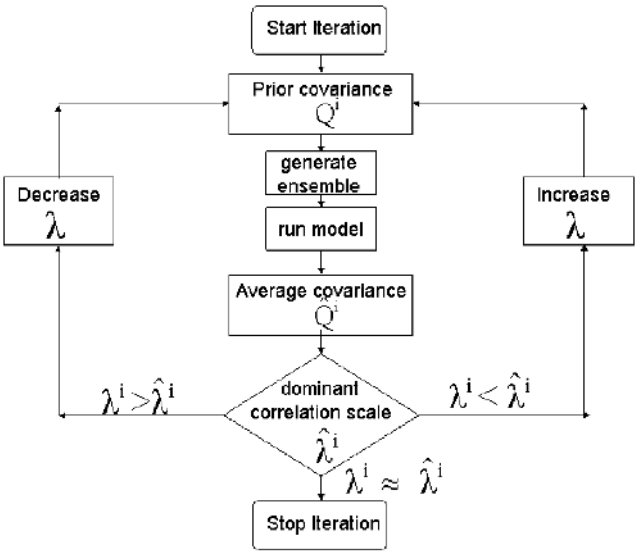

Fig. 7. Sketch of the iterative process to define the correlation scale, λ, of the system noise covariance matrix, Q

otherwise it is decreased. The iteration is repeated until the calculated correlation scale is approximately equal to the prior. An ensemble of 30 members and a time window of 30 days are used in this exercise. By averaging in time over a period of 30 days, the shorter term variations in correlation are smeared out, leaving the dominant correlations in the system (i.e. averaged over spring-neap and shorter-term tides and weather-induced variability). A similar exercise was done for the magnitude of the variance. These assumptions on the unknown structure of the system noise matrix are used in the filter as explained in section [The Ensemble Kalman Filter (EnKF)].

Finally, from these exercises, the standard deviation of the SPM concentration model error was assumed spatially variable with an average error of 2 g m^{-3} and independent in time, while the natural correlation length scale appears to be around 50 km, varying in space and in time but constant within a period of a month. An example of the uncertainty correlation scales spatial structure and the standard deviation of the system noise (i.e. model error) used in the EnKF is given in Figure 8.

Spatial mapping between model and observations

In order to assimilate the observed data into the model, spatial mapping has to be done to enable consistent comparison of the measured to modelled domain. Within data assimilation, usually, it is the model state that is

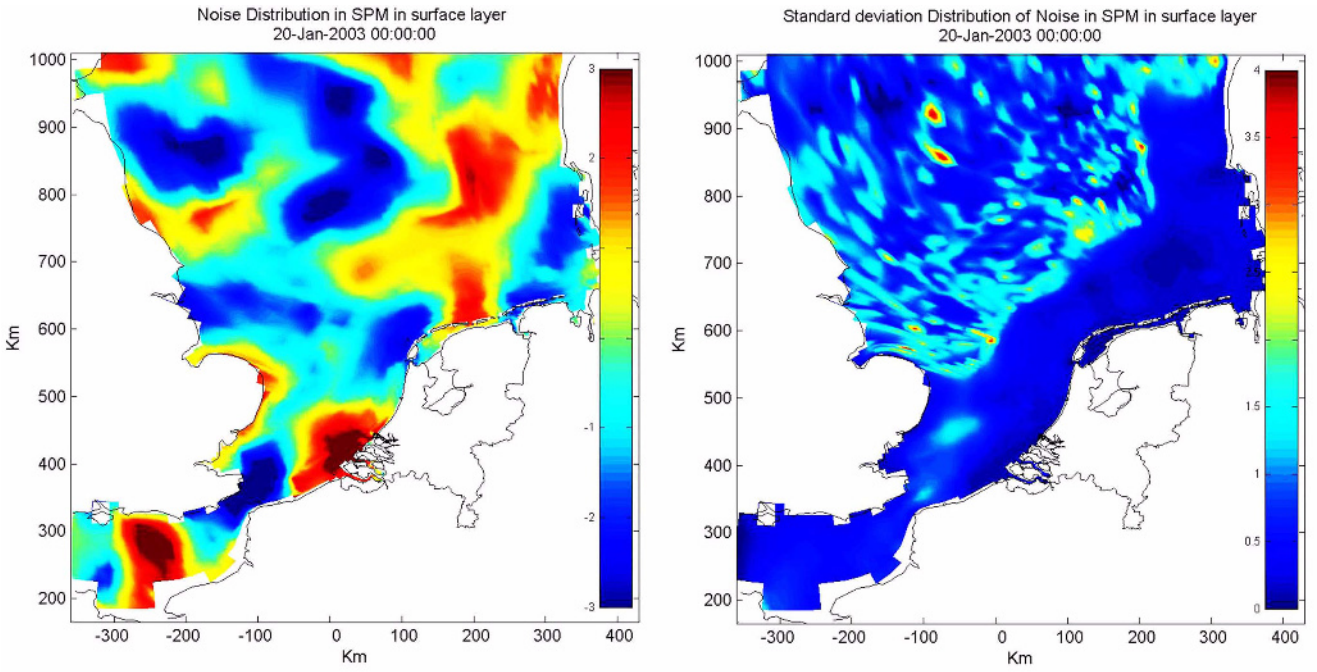

Fig. 8. Average noise distribution (left) and average noise standard deviation (right) for the month of January in gSPM m-3 used in describing the model error covariance matrix structure used in the EnKF

mapped to the data. However, in the present application that would involve too many interpolations between grid centres and measured SPM at pixel level, which would complicate the data assimilation scheme. Such mapping might also lead to redundancy in the information, since two adjacent pixels more often will share the same model grid cell. To avoid these complications, the MERIS data were mapped to the model grid. There are several choices of mapping in which the error information in the averaging may be taken into account. For the current study which mostly aims at exploring the feasibility of the assimilation, a regular spatial averaging procedure was adopted.

From comparison of the original 1 km MERIS Reduced Resolution (Figure 9) against the gridded SPM data (Figure 10), it is clear that the dominant information in the pixel data is represented in the gridded data. Meanders and eddies possibly resolved in the original data may be partly lost upon gridding. Also, when very few pixels are present

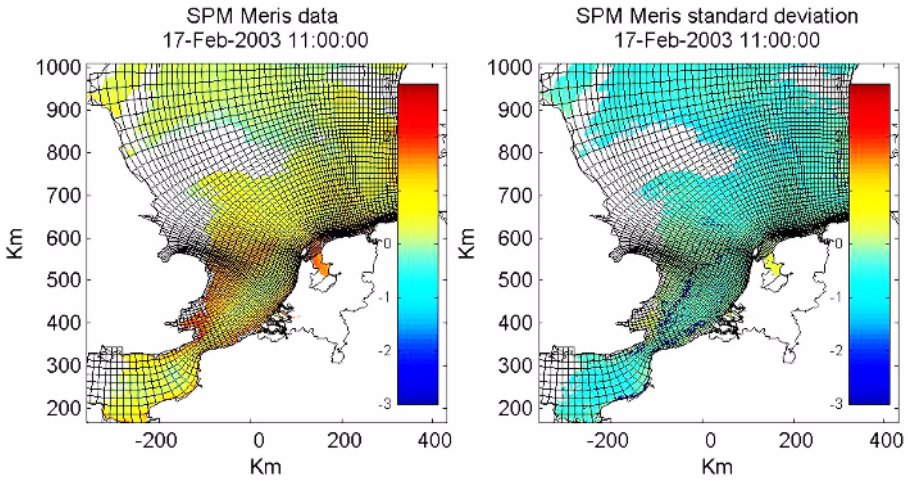

Fig. 9. SPM product MERIS data and its standard deviation "zoomed" into the area of interest on the 17th February 2003 (Addressed in the text as RAW data)

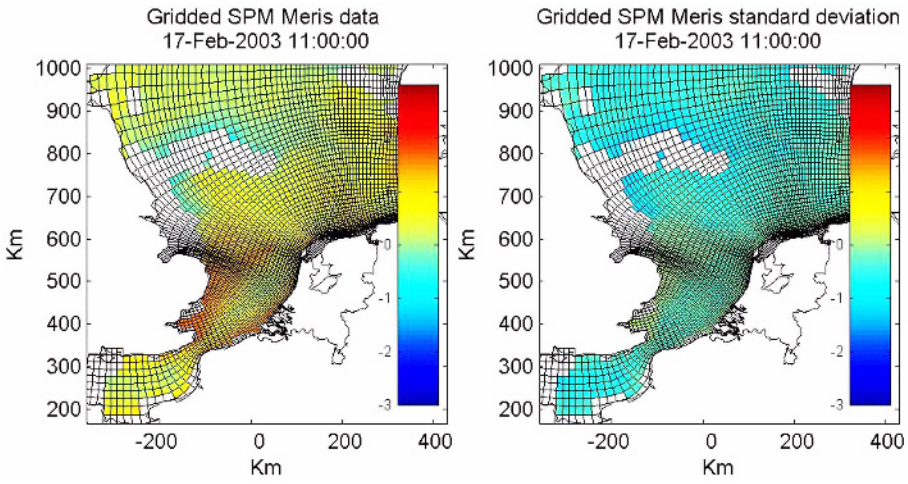

Fig. 10. Gridded SPM product from MERIS data and the standard deviation of the gridded SPM on the 17th February 2003 used in the assimilation. Only the area of interest is shown in the figure

within a single grid cell of the model, weakly representative or inaccurate results of SPM may be obtained. Also some inaccurate data coverage can be observed in the cloudy areas. This is due to the presence of one or two pixels in a mostly clouded grid cell. To avoid such artefacts, more sophisticated averaging including the number of pixels present in the cell, the error information and spatial interpolation are recommended for follow-up studies.

5. Assimilation Experiment Results

The experiment is carried out by assimilating the gridded SPM data into the model during the period of January-July 2003. The assessment on the behaviour of the filter was performed on the results of February-July, excluding January, because the results of January are considered to be affected by the spin up of the EnKF. At the beginning of the filter application, there is no prior information in the ensemble other than the error in the initial conditions. During the first month of application of the sequential filter, the effect of the initial condition and limited number of measurements might be dominant. Next, under assumption of the model and observational errors and with a successful sequential filtering, the EnKF results are expected to improve by incorporating measurements in time. Moreover, by incorporating more data every day, the difference between the model SPM prediction and the observed data will decrease but is still sufficiently large (i.e. not zero) to avoid filter divergence (Jazwinski 1970).

Verification/assessment of filter performance

Instantaneous results

As an example of instantaneous spatial results, the assimilation results on the 17th February 2003 are shown in Figure 11. Generally speaking, the assimilation results would combine the information present in both the model and the MERIS readings. The results of the assimilation are closer to the MERIS data where they are more accurate than the model and include the detailed information of the model where no data are available. The figure shows improvements along the Dutch coast, where the high SPM values better match those monitored by MERIS. On the other hand, only slight improvements in the model results are obtained in the unmeasured area on the northern English coast due to the lack of information from MERIS. Note that Figure 11 shows the results at an individual date (i.e. daily time scale), which might not be representative for the whole period.

Semi-annual statistics

To assess the effect of the EnKF on the SPM distribution, first the statistics of the solution over the entire period are discussed. Figure 12 shows the median surface concentration of SPM in both the deterministic and assimilated model next to the gridded MERIS data.

The assimilation affects the solution in the parts of the western and northern parts of the domain relatively strongly. Notably the signal from the East Anglia plume and

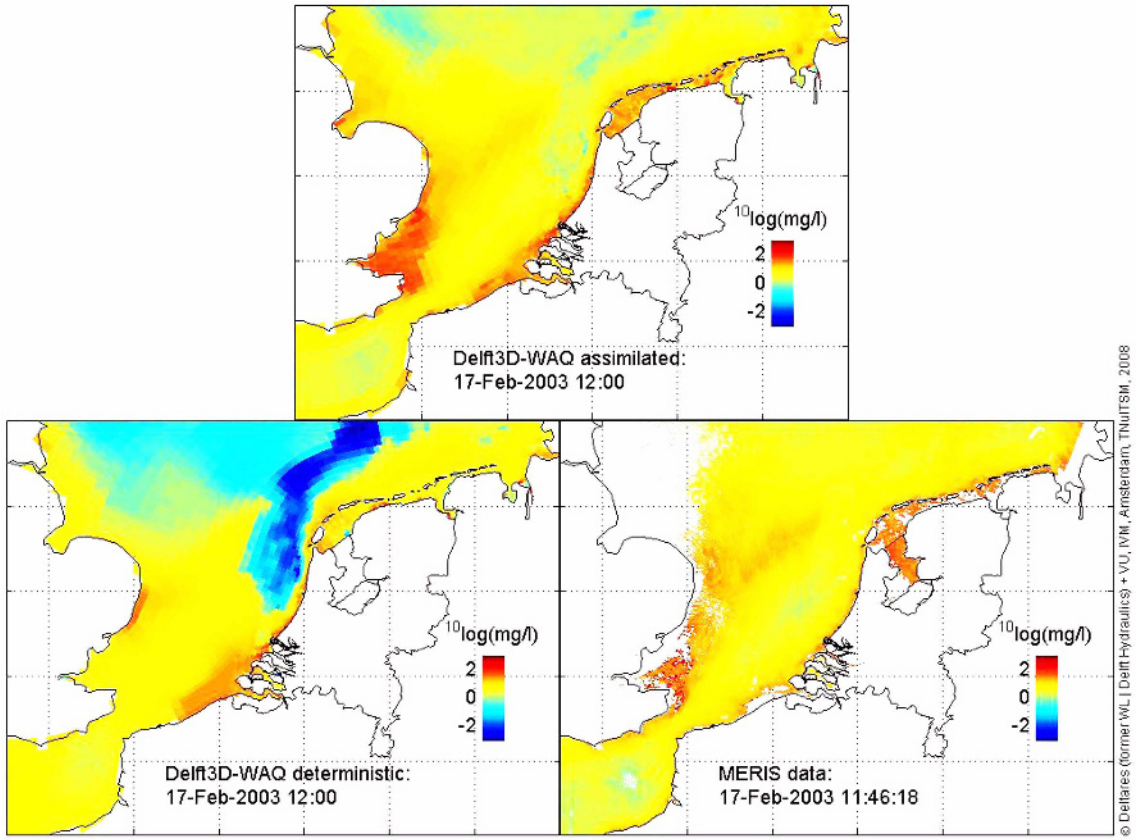

Fig. 11. Effect of assimilating MERIS data on the spatial SPM description on the 17th February 2003

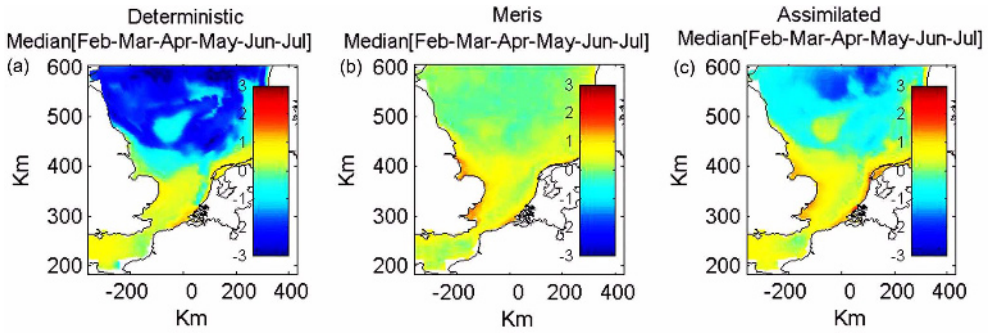

Fig. 12. SPM median of February-July 2003 (a) average deterministic model results (b) assimilated (c) MERIS gridded data

the deeper North Sea waters shows up more prominently after assimilation. This is due to a persistent difference between the retrieved (Eleveld et al. 2008; Pietrzak et al. in press) and modelled concentrations here. It indicates that the deterministic model has been designed for, and calibrated on in situ data from sites in the Dutch and Belgian sector of the domain, the area where the model resolution is highest as well (Van Kessel et al. 2010). In other words, SPM characteristics in the transport model (settling velocity, critical shear stress for resuspension) correspond more to continental than deep water or East Anglia conditions. Although the parameterisation and characteristics of the remote sensing algorithm are also calibrated to the continental conditions (Van der Woerd and Pastekamp 2008), they do show a response on the East Anglia and central North Sea waters structurally different from the transport model.

The spatial change in errors is also seen in more detail from Figure 13. It shows the differences between deterministic model and remote sensing over the entire assimilation period (i.e. residuals in the deterministic model

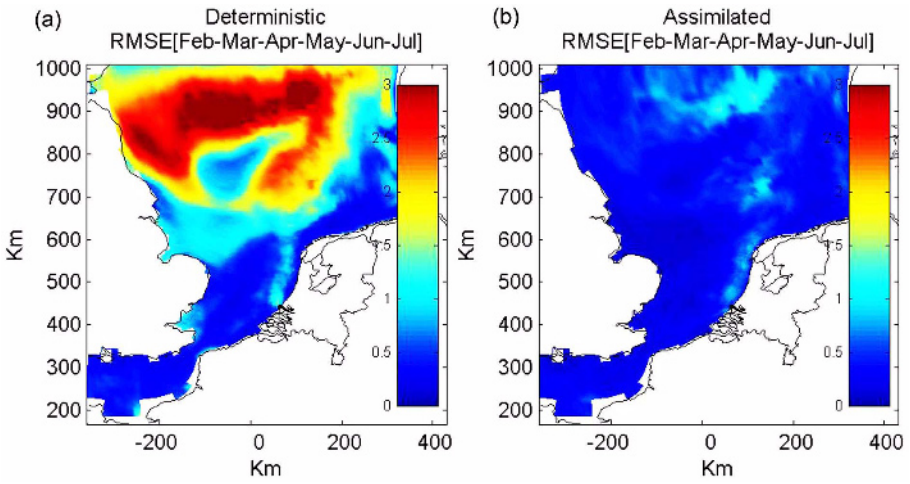

Fig. 13. SPM RMSE of February-July of 2003 for (a) deterministic model results, and (b) assimilation results

RMSE) and also the residuals (RMSE) in the assimilated SPM. The residuals decrease considerable and thus the improvement in the assimilated field is thus confirmed for the whole simulation period.

Bi-monthly statistics

Similarly the RMSE statistics test was carried out for bimonthly variation (Figure 14). In February and March where the MERIS coverage is low due to clouds, the residuals are higher than those in June-July when the coverage is higher (summer weather period). Along the Dutch coast, in February-March (mainly March), the residuals in the assimilation results are higher than those in the deterministic run. This indicates that the assimilation is not capable of improving the model description in that area under those conditions and amplifies some shortcomings of the deterministic model. These shortcomings are probably related to high-river discharge events. The freshwater outflow contributes to temporary haline stratification followed by mixing (Simpson and Souza 1995; De Boer et al. 2006; Pietrzak et al. in press). The model either overestimates the mixing within this area and/or overestimates the shear stress which is the governing force for SPM resuspension. These issues are also shown in more details in the following section.

Monthly statistics

To assess if the filter on average (at all locations and all times per month) is improving the spatial-temporal description with respect to the MERIS data, the average RMSE per month is presented for both the assimilation results (ε_{assim})

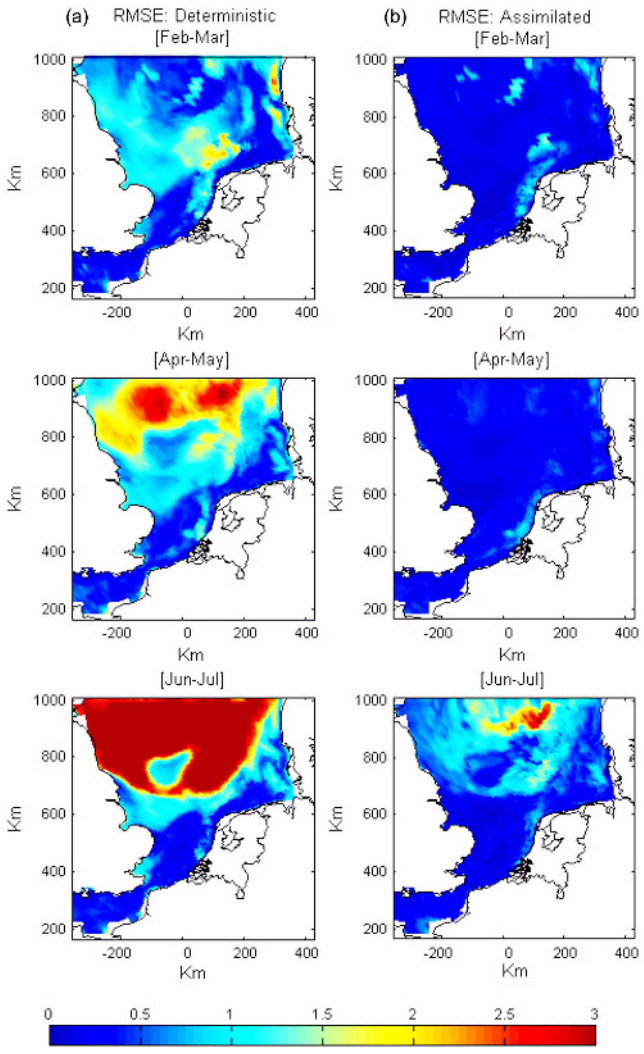

Fig. 14. SPM RMSE of bi-monthly periods from February till July of 2003 for (a) deterministic model results, and (b) RMSE assimilation results

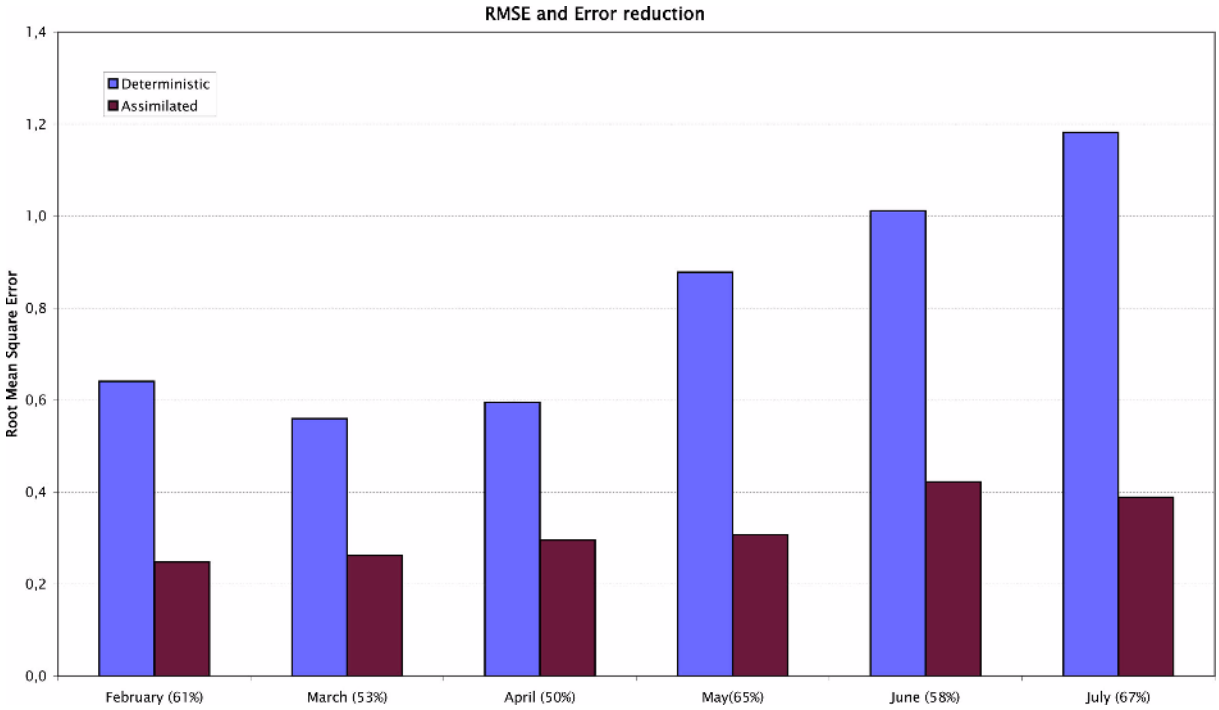

Fig. 15. SPM RMSE of monthly variation in RMSE and its error reduction percentage during period from February till July of 2003

and the deterministic results (ε_{det}) in Figure 15. Also an error reduction percentage has been calculated as follows

$$\gamma^{Meris} = \frac{(\varepsilon_{det}^{Meris} - \varepsilon_{assim}^{Meris})}{\varepsilon_{det}^{Meris}} \times 100$$

The error reduction percentage varies between 52% to 67%. On average, the residuals do confirm the success of the experiments and they show no seasonal dependence in the behaviour of the filter (Figure 15). These results are a verification of the technical feasibility of the assimilation experiment. They also confirm the feasibility of applying the data assimilation presented and the assumptions discussed in section [Error Covariance matrices structure]. The results as such only do not assess the accuracy gained in the description of SPM through data assimilation. This is done with the help of independent data (data not used in the assimilation or the calibration of the model), as presented in the following section.

Validation against *in situ* data (independent data)

Sampling biases

A validation of the assimilation results is feasible for those locations and conditions where samples have been taken. The question thus is to what degree the in situ samples are representative for a wider range of conditions and sites. By lack of a sufficiently large and equally spread spatial coverage (45 sites) we do not formally assess the spatial bias. We limit ourselves to the obvious conclusion that the statements in this study are spatially confined to the Belgian and Dutch coastal zone. Still it is worthwhile to assess the temporal behaviour of the assimilation results against the independent *in situ* data in the North Sea. The Belgian and Dutch field data that have been available are ship-borne low-frequency bottle sample observations from the national monitoring programs. The Dutch stations are organized in cross-shore transects, each transect bears the name of the closest coastal town, each station on the transect is identified by its offshore distance in km. These in situ data are almost always collected at relatively calm sea states, because of safety and data collection policies on board of the monitoring vessels (see also Fettweis and Nechad 2010). (see Figure 5 for the sampling sites; for more information, see www.mumm.ac.be/datacenter/;live. waterbase.nl)

Also the remote sensing of ocean colour of the southern North Sea may have a bias towards weather conditions with relatively lower winds and wave heights, as discussed by Fettweis et al. 2007. These constraints of satellite imagery relate to the fact that the optical satellite observations

obviously depend on clear sky conditions. The differences between in situ and remote sensing sampling strategy notwithstanding, Eleveld et al. (2008) showed that SPM in situ could be estimated from SPM remote sensing and vice versa.

To check if similar inference about the "all-weather" conditions could be made about the model results from the in situ sample set, a so-called Wilcoxon rank sum test (Mann-Whitney U-test for the medians) has been applied on two sample sets: a set sampled with the in situ sampling strategy of 2003 (given the times of all samples considered in the analysis) and the other set is sampled randomly keeping the same sample size. If the distribution of the two samples is not statistically different in terms of the relevant weather condition parameter, then the measurement strategy may be presumed to be representative for the all conditions. The relevant weather-related parameter could either be the wave conditions (i.e. wave height, since wave period does not vary widely in the southern North Sea, see also section [SPM transport Model Description]) or the bottom shear stress that is determined by the combination of (tidal) currents and waves and local depth. The combined current-wave induced bed shear stress (τ_{cw}) is the most directly weather dependent factor affecting the resuspension and vertical mixing of the SPM. Under the presumption that the statistics of the modelled bottom stresses at all sampling sites are well representing the unknown -for unmeasured- bottom stresses in the field, the statistical test is carried out on the bed shear stress in the model. The statistics of both samples are given in Table 2.

From the results it is concluded that the samples are significantly different with respect to the medians of the two distributions. Note that the same test was carried out on the significant height squared in the model domain shows no statistically significant difference from the given (limited, i.e. 6 months) sample size. The difference is explained by the fact that the distribution of bottom stresses is more skewed than that of wave height squared because the combination of square of wave height, period and depth determines the wave-induced stress (Soulsby 1997). This skewness emphasises the maxima. In summary, it is concluded that the validation to the in situ measurements is representing calm conditions. A validation of the assimilated model results under stormy conditions can only be carried out when semi-continuous measurements become available for the period and area of interest.

Time series

The results are further discussed using a selection of time series of both the deterministic and assimilated model results along with the in situ data and MERIS data mapped to the model grid. Figure 16(a) till Figure 16(g) show time series of SPM from the deterministic and assimilated model, together with the gridded MERIS data and in situ observations. In a separate panel the modelled current-wave bottom shear stress (τ_{cw}) is shown for reference. Results are shown from January onward to illustrate the effect of the filter during the spin up period as well.

All figures share the fact that assimilated and deterministic results begin to differ only after about the first 5 days as soon as the first MERIS data have become available for the assimilation procedure. Also it can be noted that some solutions start to differ slightly already before the first MERIS observations are found in their own corresponding model grid cell. This slight change is due to advection of SPM from parts of the domain that have been updated before and due to the spatial correlation that might be present in the update matrix as given in Eq. (5).

We distinguish three categories of station sites: (1) close to shore (i.e. less than approximately 5 km offshore); These are the sites where waves are most frequently capable of resuspending SPM and where the variability may also be affected by riverine water. (2) Moderate distance offshore (stations 5-20 kms, still affected by waves, less riverine influence); (3) Far offshore (>20 km) which are characterized by lower concentrations, not directly affected by wave and tidal resuspension, but still experiencing spring-neap tidal

Table 2. Statistics of the subsamples and the entire model-generated wave-current bottom shear stress. The in situ set is sampled according to the ship-borne measurements of the SPM concentrations; the random set is of same size.

Tau	In situ sample (45 stations, on average 10 samples per station)	Random sample (same size, random in time and stations)	all (model, daily samples, entire year all stations)
Mean	2.11	3.87	3.09
Median	0.83	2.02	1.73
Std	3.41	5.58	4.33
Rms	3.98	6.79	5.32

variations in mixing and advection (Eleveld et al. 2008). The sites are located in the area where the case-II North Sea waters characterization and the calibration of the HYDROPT retrieval are holding. Since the temporal sampling frequency at other stations is similarly low or even lower, it has been decided not to include all time series and discuss them at length, but to select a representative set that cover more or less successful results.

Close to shore stations

Stations such as Walcheren-2, and Huibertgat are part of the first category for which the distance varies between 2 kms to 5 kms offshore as shown in Figure 5.

At Walcheren-2, Figure 16(a), it is seen that in the first month of the assimilation, the MERIS SPM concentrations tend to be lower than the deterministic model results. This slightly lowers the assimilated concentrations, whereas in the later half of the period an increase of concentrations is found. The effect appears to be strongest in April in line with a larger difference between the deterministic run and the MERIS data in that period. The in situ data - though low in frequency- are consistent with the assimilated result.

The Huibertgat data as in Figure 16(b) show a general under-prediction of the deterministic model with respect to both MERIS data and in situ data until April. Due to assimilation, the assimilation is inducing a clear positive offset and an increase in the range of variations. The MERIS data tend to show a higher mean than the in situ data during

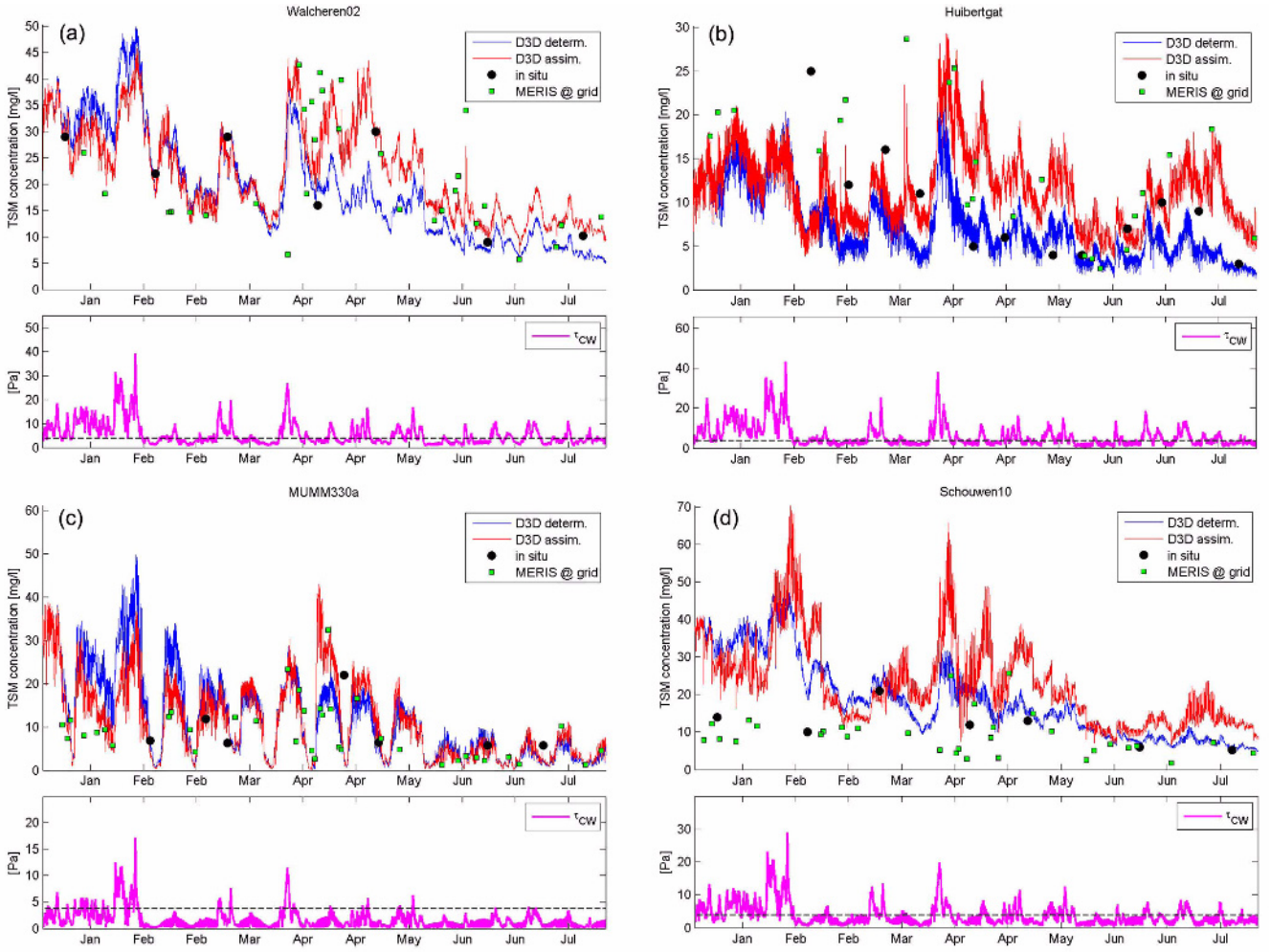

Fig. 16. Time series of surface concentration at selected in situ stations (cf. Figure 5) for the period of January-July 2003. Deterministic model results blue, assimilated model results red, MERIS data as used in the assimilation green, independent in situ data black (top panels), Bottom panels show modelled current-wave bottom shear stress as indicator of local resuspension and vertical mixing. Dashed line indicates critical threshold for bed mobilisation in the model. (a) Wacheren 2, (b) Huibertgat., (c) MUMM 330a, (d) Schouwen 10, (e) Noordwijk 10, (f) Noordwijk 70, (g) Terschelling 100

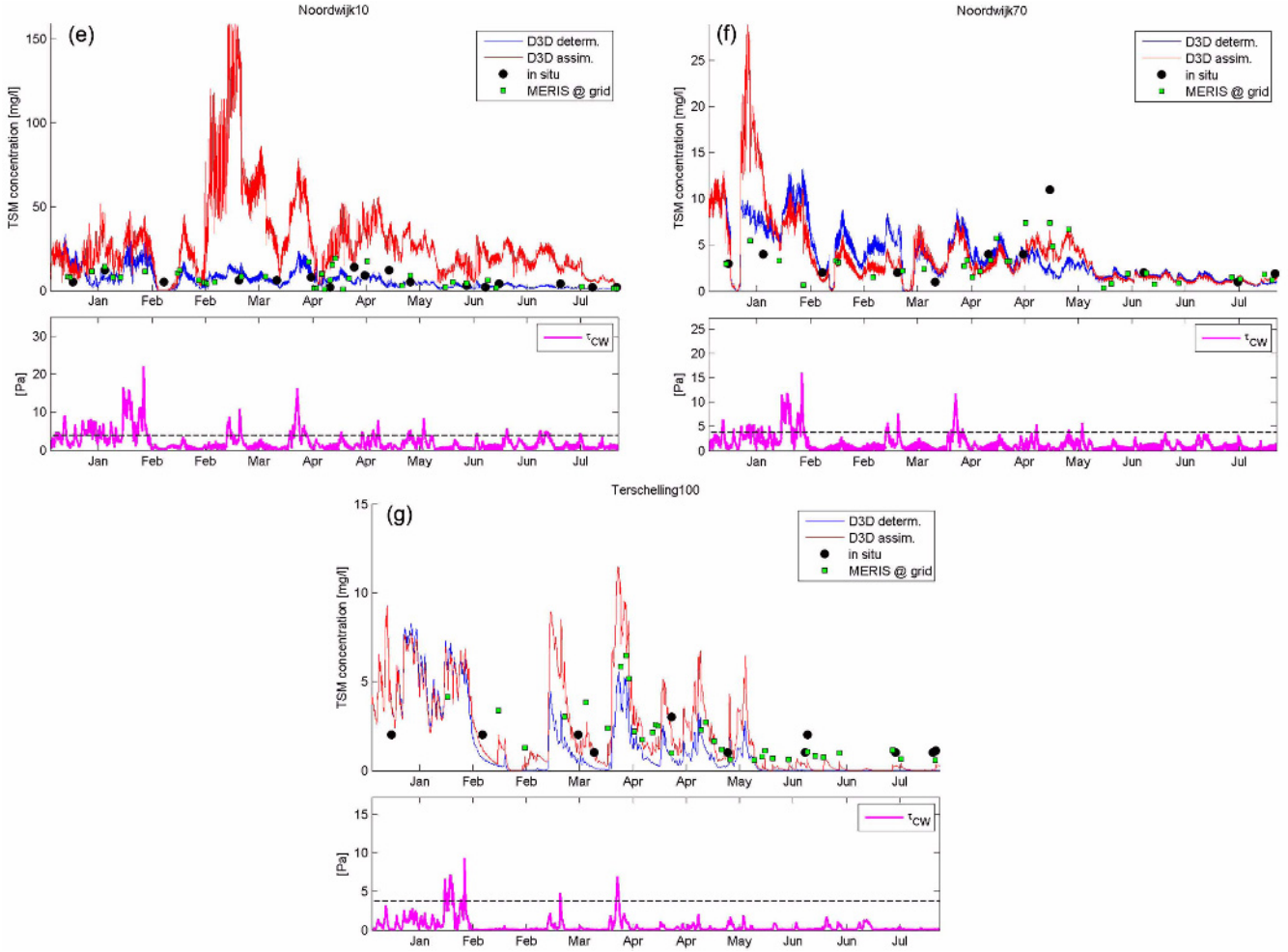

Fig. 16. (continued)

spring and the period thereafter. The assimilation of those high values kept the mean of the SPM assimilation results higher than the deterministic model SPM throughout the rest of the period.

Moderately nearshore stations

The stations such as MUMM 330a, Schouwen 10, Noordwijk 10 are moderately nearshore with water depths of 10 to 20 m.

The MUMM 330a station (Figure 16(c)) is characterised by a clear spring-neap tidal resuspension pattern (Van der Wal et al. 2010). This station is relatively closely situated near the Flemish Banks which are considered a source of SPM (Fettweis et al. 2007). In the model this source strength is unaffected by the assimilation and consequently the assimilation has only a modest effect on the average concentrations in this area. Nevertheless, the amplitude of the spring-neap variations appears generally controlled by the amplitude of the fluctuations of the MERIS data on the spring-neap tidal time scale. The assimilated concentrations are generally lower than the deterministic, except in late April-early May when the MERIS data tend to be higher than average.

The Schouwen 10 station is a site where the deterministic model seems to overestimate the concentrations (Figure 16(d)), and after assimilation this overestimation has even increased. This area is under influence of the outflow of river water of the Rhine-Meuse system through the Haringvliet sluices (Figure 15). The model as such tends to overestimate the SPM concentrations, presumably because it overestimates the vertical mixing in this estuarine region. The assimilation tends to amplify the model shortcomings here.

Noordwijk 10 (Figure 16(e)) is the station where the deterministic model traditionally tends to perform best in annual mean sense. The parameter values in the erosion and

deposition parameterization of the mixed sand-mud bed tend to be biased towards the Noordwijk conditions 5 to 10 km offshore for historic reasons such as relatively high data availability and incidental past high-frequency measurement campaigns such as reported by Hartog and Van de Kreeke 2003. The development of the sand-mud mixture model in Delft3D WAQ has been strongly based on high-frequency Smart Mooring data in the years 2000-2002 at these Noordwijk sites (Van Kessel et al. 2010).

Notably, the assimilation does not improve the model results here. This is, however, only partly due to the aforementioned bias of the deterministic model towards this site. More importantly, the nearshore stations of Noordwijk are representing a highly dynamic area due to the relatively strong influence by the outflow of Rhine-Meuse rivers. In this Region of Fresh water Influence (ROFI) the freshwater outflow contributes to periods of haline stratification followed by destratification depending on spring-neap and semidiurnal tidal phase and wind and wave induced mixing (e.g. Simpson and Souza 1995; De Boer et al. 2006). Hence, the shortcomings reported above at Schouwen10 in the model and assimilation to deal with the episodic stratification/ destratification adversely affects the assimilation. This indicates the complexity of the hydrodynamics in the area (Fettweis et al. 2009; van den Eynde 2004). In general the result is an overestimation of assimilated SPM that only occasionally is corrected with assimilation of low values of MERIS data. In particular, the increase in surface salinity shown in Figure 16(b) at the end of February coincides with the steep increase of SPM in that period in Figure 16(e).

Due to lack of observations of vertical profiles of salinity and SPM it is not possible to assess in detail to what degree the transport model is capable of describing these events and to what extent and how the assimilation in turn depends on the vertical structure of the modelled water column. Further research should be dedicated to identify the sources of the overshooting.

Offshore Stations

Noordwijk 70, and Terschelling 100 are further offshore stations at water depths of about 30 to 40 m.

Noordwijk 70 (Figure 16(f)) shows a relatively moderate response consistent with the values of both the MERIS data and the in situ data. In general the assimilated results tend to be lower than the deterministic. Two exceptions are the peak in January which can be related to the river outflow event (Figure 6(a,b)) and an increase in April-May values both in remote sensing and in situ data, that has been observed at other stations discussed here as well. This quite persistent mismatch between model and both MERIS and in situ data suggests that the effect of the phytoplankton spring bloom and the subsequent increase of the organic compound of SPM may be playing a role (Wild-Allen et al. 2002; McCandliss et al. 2002).

Terschelling 100 (Figure 16(g)) is characterised by even lower concentrations and smaller absolute variations. In the winter months there are too few observations both form MERIS and in situ to affect the assimilation and validate the response. In spring however, the assimilation results show a remarkable temporal pattern of a bi-weekly steep increase and gradual decrease that is also present in the MERIS data with slightly larger amplitude than the deterministic model. The comparison with the bottom shear stress suggests that the peaks are not directly determined by resuspension when the stresses exceed critical level (which only occasionally occurs at this site). Inspection of the spatial patterns in the model results show that the saw-tooth behaviour can be related to increases in the eastward extent of the East Anglian Plume towards the area of Terschelling 100 during high shear stress periods and a gradual relaxes afterwards. Hence, the patterns in this area are influenced more by advection and vertical wind-induced mixing. The fact that the elevated peaks start before the local shear stress increases indicates that material is advected from more exposed areas and/or mixed from lower water layers. Once mixing decreases the material gradually settles. Unfortunately, the frequency in situ data is insufficient to corroborate these suggested mechanisms.

Overall assessment

All available in situ measurements at the 45 applicable stations in the area were included in Figure 17 against its corresponding deterministic value and assimilated value. The MERIS data were also included. The MERIS data however have been included within a time window of ±6 hours and following the same mapping as presented in section [Spatial mapping between model and observations] (i.e. averaged value of all pixels within the grid cell). The results in the figure show that there are no systematic biases in the assimilation run (overestimation or underestimation). Compared to the deterministic run or the MERIS reading, they are better matching the in situ data (on 45° line). Due to

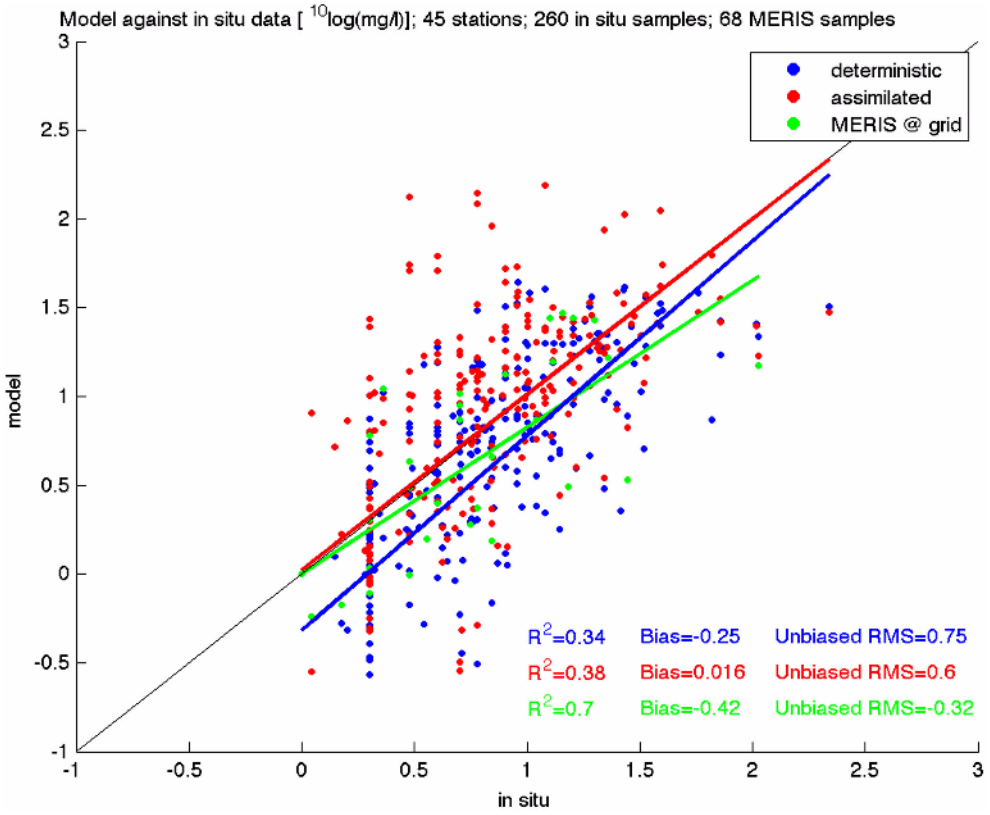

Fig. 17. Scatter diagram of SPM concentration of the deterministic run (blue), assimilated run (red) and the MERIS data (green) against the in situ data. The lines are linear regression line with the corresponding colour to its data set. The thin black line is the 1:1 line

assimilation, the mismatch of the deterministic results to the insitu measurements (bias) is clearly reduced whereas the unbiased RMS value and R^2 (both indicative of the variance matching) have been marginally improved. The validation against independent measurements that are not used in the experiment (i.e. insitu measurement) viewed in Figure 17 across all stations collectively, confirms that the SPM as a result of the assimilation is better described.

To represent the improvement achieved by the assimilation in a statistical comparison, the average RMS error (RMSE) in the deterministic SPM with respect to dependent and independent measurements is compared to that of the assimilated SPM for all stations and is presented in Table 3. The RMSE error is presented with respect to the MERIS data (dependent data) to ensure the good performance of the filter and to the in situ data (independent data) to present the validation of the improvement. The average RMSE, $\varepsilon_{det}^{Meris}$, of the deterministic results is the RMSE based on the difference between the deterministic and the MERIS data and averaged over all stations at all instances of MERIS

Table 3. Average absolute error in the deterministic SPM and the estimated SPM (assimilated) relative to the MERIS data and the in situ independent data and the percentage reduction in the error due to the assimilation

	absolute error (mg/l)		% reduction in absolute error
	deterministic	assimilation	%
MERIS	10,85	9,30	13,92
in situ	8.93	8.00	10.41

readings within the period of the experiment. Similarly, the averaged RMSE in the estimated SPM due to assimilation $\varepsilon_{assim}^{Meris}$ is also calculated. The average RMSE, $\varepsilon_{det}^{insitu}$ of the deterministic results and that of the assimilated results, $\varepsilon_{assim}^{insitu}$, compared with the insitu measurements is also presented. As in section [Monthly statistics], the percentage reduction in the error is calculated with respect to the independent in situ data. Due to assimilation, 13.92% of the error in the deterministic model was reduced with respect to MERIS data. That means that the estimate of the SPM through assimilation is closer to the MERIS data than the

deterministic SPM without assimilation. This means that the assimilation scheme seem overall to be quite successfully implemented. With respect to the in situ data, a reduction of 10.41% of the error has been achieved. The in situ data are independent data and not used in the assimilation and they are also considered to be more accurate in nature. Obviously, the assimilation results are closer to the in situ data than the deterministic model.

6. Conclusions and Recommendations

In this paper, the deterministic DELFT3D-WAQ sediment transport and water quality model is extended with an Ensemble Kalman filter (EnKF) technique that enables generic assimilation of recent observational data of SPM products retrieved from the MERIS reflectance measurements. The techniques are demonstrated for SPM prediction in the southern North Sea. These first results of the assimilation of MERIS-derived SPM into Delft3D-WAQ are encouraging. Many new aspects related to the assimilation of SPM remote sensing data in numerical models such as the spatial mapping, the uncertainty definition, the definition of the optical depth, have been identified during this research. The data assimilation seems to be able to handle the spatial-temporal variability of SPM. We observe that the generic filter is robust and stable. Given the presumptions on ensemble sizes, structure of the covariance matrices and mapping of observations to model, the results of the assimilation experiment are certainly promising. There are issues however that are still open for discussion and/or require further investigation.

Ensemble size

In the data assimilation, an ensemble size of 30 members was used which may be a quite limited number of members. A test was carried out by increasing the number of ensemble members to 50 and to 100 for a few days of the assimilation and the results were roughly comparable to those of 30 ensembles (not presented here). However, the computational burden to continue the rest of the assimilation experiment with those ensemble sizes was prohibitive. Hence, it was concluded that increasing the number of members would only marginally improve the results and enhance them at a major cost. Still, a more extensive study of the ensemble size with extended computational resources might be recommended.

Model error covariance matrix

Spatial correlation scales of 50 km resulted from an iterative procedure in the construction of the model error covariance matrix. The results of this procedure however suggest that there may be anisotropy in the error correlation length scale depending on the residual current pattern: in the offshore central part of the domain length scales can be isotropic and of the order of 30 km, whereas in the nearshore along and across streamline length scales differ strongly (well over 50 km, to about 10 km respectively). Hence, the present assumptions on the uncertainty structure of the model errors are to be considered as a compromise. Although persistent natural correlation scales and varying standard deviation have been used in this paper (cf. section [Error Covariance Matrix Structure]), they are to be considered at this stage the best guess of system noise. The analysis of those topics will be carried out more thoroughly and will be presented in a follow up paper. It is expected that this will improve the results of the assimilation. Comparison of assimilation results due to different assumptions to independent set of data (i.e. in situ measurements) is also recommended as a further verification step for the assumption on the uncertainties structure.

Improve mapping between model and remote sensing data

Observations from space are limited to the surface layer. Ninety percent of the light exiting the water column comes from one unit optical depth, while the numerical model deals with the suspended particulate matter concentration over the entire depth of the water column. To be able to compare and assimilate the observed SPM concentration into the model, one has to match the representative portions of the water column and use the equivalent depths in both domains. In this experiment, this was not taken into consideration, as the depth of the first sigma layer of the model was assumed to equal the optical depth observed. This means that we assumed that the SPM concentrations observed by the MERIS instrument are equivalent to the predicted SPM concentration in the surface layer of the numerical model. Where the assumption is invalid, this can create inconsistencies. Additional optical depth information needs to be incorporated in the assimilation to eliminate and/or decrease this mismatch.

Extend in time, include newly collected data

From the experiments discussed here, we conclude that

the EnKF can be successfully applied. The procedure seems suited to reach a solution that is consistent not only with the model equations, but also with general notions of the coastal system. Using a 3D transport model enables the interpolation in horizontal (underneath clouds) and time (between overpasses). Applying this type of data assimilation for an entire year or even multiple years will extend the description of the coastal system in a physically consistent way. Nevertheless, more extensive investigation of and validation against *in situ* data is recommended. Recently, new cruise data are becoming available for the southern North Sea that covers not only the surface layer but the entire vertical profile at over 50 stations. These data are especially useful to evaluate the vertical structure of the model results. In addition, high time-resolution time series of semi-permanent moorings and ferry boxes are being made available which allow investigating and validating the temporal patterns further (e.g. Petersen et al. 2008; Kröger et al. 2009).

Improve model

Once new data are available it is recommended to first improve the deterministic model as such. Further studies of the complex stratification/de-stratification processes in particular in the Rhine ROFI and the required vertical and horizontal model resolution to describe these processes sufficiently accurate are highly recommended. Also the number of SPM fractions, the model coefficient setting and the lack of explicit organic material in the model are issues to further investigate.

Model skill assessment

A final step is then an objective quantitative assessment of the improvements in model skill obtained by application of the data assimilation. For this, we for example plan to adopt methods presented by Taylor (2001) who devised an objective measure for model skill depending on standard deviations of model and validation data, model-data correlation coefficient and the maximum potentially achievable correlation given the stochastic nature of the solution. Since the spatial-temporal scales of SPM in the coastal zone vary widely and stochastic patterns may be found that can only partly be resolved by the numerical models, a limit is to be expected as to what goodness of fit is achievable at all. In order to fully assess the value of the data-assimilation as described above, a follow-up study is recommended in which different periods in time are to be simulated and validated against field data currently collected by the Port of Rotterdam.

Acknowledgments

The authors gratefully acknowledge the financial support by The Netherlands Agency for Aerospace Research (NIVR) User Support Program, Grant GO 2005/50 (53618WL) and the sponsoring and participation by the Port of Rotterdam. They also kindly acknowledge the financial support provided for this project by the Ministry of Economic Affairs within the framework of the WL | Delft Hydraulics R&D Program (*Doelsubsidie EZ*) and the Delft Cluster research project 'Sustainable development of North Sea and Coast', DC-05.20. 9. The authors are thankful to ESA for provision of data. We thank Reinold Pasterkamp for the HYDROPT software library, Steef Peters for MEGS7.4 optimization, and Gerben de Boer and Jan van Beek for sharing their valuable experience. Bram van Prooijen (Delft Technical University) is acknowledged for sharing his work on the integration of wave buoy data and SWAN model results. Finally, the input and advice of Wil Borst, on behalf of the Port of Rotterdam and valuable experience and comments by Onno van Tongeren (*Data Analyse Ecologie*, Arnhem) during the research are gratefully acknowledged.

Reference

Allen JI, Holt JT, Blackford J, Proctor R (2007) Error quantification of a high-resolution coupled hydrodynamic ecosystem coastal-ocean model: Part 2. Chlorophyll-a, nutrients and SPM. J Mar Sys **68**(3-4):381-404. doi:10.1016/j.jmarsys.2007.01.005

Baumert H, Chapalain G, Smaoui H, McManus JP, Yagi H, Regener M, Sündermann J, Szilagy B (2000) Modelling and numerical simulation of turbulence, waves and suspended sediments for pre-operational use in coastal seas. Coast Eng **41**(1-3):63-93. doi:10.1016/S0378-3839(00)00027-2

Chen C, Malanotte-Rizzoli P, Wei J, Beardsley RC, Lai Z, Xue P, Lyu S, Xu Q, Qi J, Cowles G (2009) Comparison and validation of Kalman filters for coastal ocean problems: an experiment with FVCOM. J Geophys Res **114**:C05011. doi:10.1029/2007JC004548

De Boer GJ, Pietrzak JD, Winterwerp JC (2006) On the vertical structure of the Rhine region of freshwater influence. Oce Dyn **56**:198-216. doi:10.1007/s10236-005-0042-1

De Boer GJ, Pietrzak JD, Winterwerp JC (2009) SST observations of upwelling induced by tidal straining in the Rhine ROFI. Cont Shelf Res **29**(1):263-277. doi:10.1016/j.csr.2007.06.011

Delhez EJM, Damm P, de Goede E, de Kok J, Dumas F, Gerritsen H, Jones JE, Ozer J, Pohlmann T, Rasch PS, Skogen M, Proctor R (2004) Variability of shelf-seas hydrodynamic models: lessons from the NOMADS2 project. J Mar Sys **45**(1-2):39-53. doi:10.1016/j.jmasys.2003.09.003

Dobrynin M, Gayer G, Pleskachevsky A, Günther H (2010) Effect of waves and currents on the dynamics and seasonal variations of suspended particulate matter in the North Sea, J Mar Sys **82**(1-2): 1-20. doi:10.1016/j.jmarsys.2010.02.012

Doerffer R, Fischer J (1994) Concentrations of chlorophyll, suspended matter, and gelbstoff in case II waters derived from satellite coastal zone color scanner data with inverse modeling methods. J Geophys Res **99**:7457-7466. doi:10.1029/93JC02523

Doerffer R, Schiller H (2007) The MERIS case 2 water algorithm. Int J Remote Sens **28**:517-535. doi:10.1109/TGRS.2005.848410

El Serafy GY and Mynett A (2008), Improving the operational forecasting system of the stratified flow in Osaka Bay using an ensemble Kalman filter–based steady state Kalman filter, Water Res Res, **44**(w6416):19. pp. doi:10.1029/ 2006wr005412

Eleveld MA, Pasterkamp R, van der Woerd HJ, Pietrzak JD (2008) Remotely sensed seasonality in the spatial distribution of sea-surface suspended particulate matter in the southern North Sea. Estuar Coast Shelf Sci **80**(1):103-113. doi: 10.1016/j.ecss.2008.07.015

Eleveld MA, van der Woerd HJ, Blaas M, El Serafy GY (2007) Using SPM observations derived from MERIS reflectances in a data assimilation scheme for sediment transport in the Dutch coastal zone. In: Proc. Joint 2007 EUMETSAT Meteorological Satellite Conference and the 15th American Meteorological Society. Satellite Meteorology & Oceanography Conference, Darmstadt

ESA (2006) MERIS Product handbook. Issue 2.0 (14 Apr 2006). http://envisat.esa.int/handbooks/MERIS/

Evensen G (1994) Sequential data assimilation with a nonlinear quasigeostrophic model using Monte Carlo methods to forecast error statistics. J Geophys Res **99**(C5):10143-10162. doi:10.1029/94JC00572

Evensen G (2003) The Ensemble Kalman Filter: Theoretical formulation and practical implementation. Ocean Dyn **53**:343-367. doi:10.1007/s10236-003-0036-9

Fettweis M, Nechad B, Van den Eynde D (2007) An estimate of the suspended particulate matter (SPM) transport in the southern North Sea using SeaWiFS images, in situ measurements and numerical model results. Cont Shelf Res **27**:1568-1583. doi: 10.1016/j.csr.2007.01.017

Fettweis MP, Nechad B (2010) Evaluation of in situ and remote sensing sampling methods for SPM concentrations, Belgian continental shelf (southern North Sea). Ocean Dyn. doi:10.1007/s10236-010-0310-6

Fettweis M, Houziaux JS, Four ID, Lancker VV, Baeteman C, Mathys M, Van den Eynde D, Francken F, Wartel S (2009) Long-term influence of maritime access works on the distribution of cohesive sediments: analysis of historical and recent data from the Belgian nearshore area (southern North Sea). Geo-Mar Lett **29**(5):321-330. doi:10.1007/s00367-009-0161-7

Garver SA, Siegel DA (1997) Inherent optical property inversion of ocean color spectra and its biogeochemical interpretation. 1. Time series from the Sargasso Sea. J Geophys Res **102**: 18607-18625. doi:10.1029/96JC03243

Gerritsen HG, Vos RJ, Van der Kaaij Th, Lane A, Boon JG, (2000) Suspended sediment modelling in a shelf sea (North Sea). Coast Eng **41**(1-3):317-352. doi:10.1016/S0378-3839(00)00042-9

Gordon HR, McCluney WR (1975) Estimation of the depth of sunlight penetration in the sea for remote sensing. Appl Optics **14**:413-416. doi:10.1364/AO.14.000413

Hartog, J, Van de Kreeke J (2003) Analysis of Optical Back Scatter data observed by the Smart Buoy at the stations Noordwijk 10, Noordwijk 5 and Noordwijk 2. Internal report RIKZ, Ministry of Public Works, Netherlands

Jazwinski AH (1970) Stochastic Processes and filtering theory, Academic press Inc

Keppenne C, Rienecker MM, Kurkowski NP, Adamec DD (2005) Ensemble Kalman filter assimilation of altimeter and temperature data with bias correction and application to seasonal prediction. Nonlinear Proc Geophys **12**:491-503

Klamer JC, Leonards PEG, Lamoree MH, Villerius LA, Akerman JE, Bakker JF (2005) A chemical and toxicological profile of Dutch North Sea surface sediments. Chemosphere **58**(11):1579-1587. doi:10.1016/j.chemosphere.2004.11.027

Kröger S, Parker ER, Metcalfe JD, Greenwood N, Forster RM, Sivyer DB, Pearce DJ (2009) Sensors for observing ecosystem status. Ocean Sci **5**:523-535

Laane RWPM, Sonneveldt HLA, Van der Weyden AJ, Loch JPG, Groeneveld G (1999) Trends in the spatial and temporal distribution of metals (Cd, Cu, Zn and Pb) and organic compounds (PCBs and PAHs) in Dutch coastal zone sediments from 1981 to 1996: A model case study for Cd and PCBs. J Sea Res **41**(1-2):1-17. doi:10.1016/S1385-1101(98)00038-0

Lesser GR, Roelvink JA, van Kester J AT M, Stelling GS (2004) Development and validation of a three-dimensional morphological model. Coast Eng **51**(8-9):883-915. doi 10.1016/j.coastaleng.2004.07.014

Los FJ, Tatman S, Minns AW (2004) Flyl-nd - A Future Airport in the North Sea? An Integrated Modelling Approach for Marine Ecology. In: Liong, Phoon & Babovic (eds) 6th International Conference on Hydroinformatics. World Scientific 2004

Maritorena S, Fanton d'Andon O, Mangin A, Siegel DA (2010) Merged Satellite Ocean Color Data Products Using a Bio-Optical Model: Characteristics, Benefits and Issues. Remote Sens Environ **114**(8):1791-1804. doi:10.1016/ j.rse.2010.04.002

Maritorena S, Siegel DA, Peterson A (2002) Optimization of a semianalytical ocean color model for global-scale applications. Appl Optics **41**(15):2705-2714. doi:10.1364/AO.41.002705

McCandliss RR, Jones SE, Hearn M, Latter R, Jago CF (2002) Dynamics of suspended particles in coastal waters (southern North Sea) during a spring bloom. J Sea Res **47**(3-4):285-302. doi:10.1016/S1385-1101(02)00123-5

McQuatters-Gollop A, Raitsos DE, Edwards M, Pradhan Y, Mee LD, Lavender SJ, Attrill MJ (2007) A long-term chlorophyll data set reveals regime shift in North Sea phytoplankton biomass unconnected to nutrient trends. Limnol Oceanogr **52**(2):635-648

Mobley CD, Sundman LK (2001) Hydrolight 4.2: Users' guide. Sequoia Scientific, Redmond, WA, USA. http://www.sequoiasci.com/products/Hydrolight.aspx

MUMM (2008) Belgian Marine Data Centre. http://www.mumm.ac.be/datacentre/

Peters SWM, van der Woerd HJA, Eleveld MA (2008) Ovatie-2 Final report. IVM report, Amsterdam

Pietrzak JD, de Boer GJ, Eleveld MA (2011) Mechanisms controlling the intra-annual meso-scale variability of SST and SPM in the southern North Sea. Cont Shelf Res (in press)

Postma L, Hervouet J-M (2008) Compatibility between finite volumes and finite elements using solutions of shallow water equations for substance transport. Int J Num Meth Flu **53**:1495-1507. doi:10.1002/fld.1373.

Petersen W, Wehde H, Krasemann H, Colijn F, Schroeder F (2008) FerryBox and MERIS - Assessment of Coastal and Shelf Sea Ecosystems by Combining In-situ and Remote Sensed Data Estuarine. Coast Shelf Sci **77**(2):296-307. doi:10.1016/j.ecss.2007.09.023

Press WH, Vetterling WT, Teukolsky SA, Flannery BR (1992) Numerical recipes in Fortran: The art of scientific computing, 2nd edn. In: Modelling of data. Cambridge University Press, New York, pp 650-700

Rijkswaterstaat (2008) Waterbase. http://live.waterbase.nl

Robinson AR, Lermusiaux PFJ (2002) Data assimilation for modelling and predicting coupled physical-biological interactions in the sea. In: Robinson AR, McCarthy JJ, Rothschild BJ (eds) The Sea, Wiley, New York, pp 475-535

Ruddick K, Ovidio F, Rijkeboer M (2000) Atmospheric correction of SeaWiFS imagery for turbid coastal and inland waters. Appl Optics **39**(6):97-912. doi:10.1364/AO.39.000897

Ruddick KG, De Cauwer V, Park Y-J (2007) Seaborne measurements of near infrared water-leaving reflectance: The similarity spectrum for turbid waters. Limnol Oceanogr **51**(2):1167-1179

Simpson JH, Souza AJ (1995) Semidiurnal switching of stratification in the region of freshwater influence of the Rhine. J Geophys Res **100**(C4):7037-7044. doi:10.1029/95JC00067

Soulsby R (1997) Dynamics of Marine Sands: A Manual for Practical Applications. Thomas Telford, London, 249 p

Stelling GS, van Kester JAThM (1994) On the approximation of horizontal gradients in sigma co-ordinates for bathymetry with steep bottom slopes. Int J Num Meth Flu **18**(10):915-935. doi:10.1002/fld.1650181003

Stronkhorst J, Ariese F, van Hattum B, Postma JF, de Kluijver M, Den Besten PJ, Bergman MJN, Daan R, Murk AJ Vethaak AD (2003) Environmental impact and recovery at two dumping sites for dredged material in the North Sea. Environ, Pollut **124**:17-31. 10.1016/S0269-7491(02)00430-X

Stroud JR, Stein ML, Lesht BM, Schwab DJ, Beletsky D (2010) An Ensemble Kalman Filter and Smoother for Satellite Data Assimilation, J Am Stat Ass. **105**(491):978-990. doi:10.1198/jasa.2010.ap07636

Taylor KE (2001) Summarizing multiple aspects of model performance in a single diagram, J Geophys Res **106**(D7):7183-7192. doi:10.1029/2000JD900719

Testut C-E, Brasseur P, Brankart J-M, Verron J (2003) Assimilation of sea-surface temperature and altimetric observations during 1992-1993 into an eddy-permitting primitive equation model of the North Atlantic Ocean. J Mar Syst **40-41**:291-316

Tilstone GH, Peters SWM, van der Woerd HJ, Eleveld MA, Ruddick K, Krasemann H, Schoenfeld W, Martinez-Vicente V, Blondeau-Patissier D, Doerffer R, Høkedal J, Jorgensen PV, Pasterkamp R, Röttgers R, Shutler J, Sørensen K, Astoreca R (2011) Variability in absorption properties and the performance of satellite ocean colour algorithms in North Sea Coastal Waters. J Geophys Res (Submitted)

Van Beusekom JEE, Brockmann UH, Hesse K-J, Hickel W, Poremba K, Tillmann U (1999) The importance of sediments in the transformation and turnover of nutrients and organic matter in the Wadden Sea and German Bight Dtsch Hydrogr Z./Germ. J Hydrogr **51**(2/3):245-266

Van den Eynde D (2004) Interpretation of tracer experiments with fine-grained dredging material at the Belgian Continental Shelf by the use of numerical models, J Mar Sys **48**(1-4):171-189

Van der Wal D, Van Kessel T, Eleveld MA, Vanlede J (2010) Spatial heterogeneity in estuarine mud dynamics. Ocean Dyn **60**(3):519-533. doi:10.1007/s10236-010-0271-9

Van der Woerd HJ, Pasterkamp R (2008) HYDROPT: A fast and flexible method to retrieve chlorophyll-a from multispectral satellite observations of optically complex coastal waters. Remote Sens Environ **112**:1795-1807. doi 10.1016/j.rse.2007.09.001

Van Gils JAG, Ouboter MRL De Rooij MN (1993) Modelling of water and sediment quality in the Scheldt Estuary Neth J Aquat Ecol **27**(2-4):257-265

Van Kessel, T, Winterwerp JC, Van Prooijen, BC, Van Ledden,

M, Borst WG (2010) Modelling the seasonal dynamics of SPM with a simple algorithm for the buffering of fines in a sandy seabed. Cont Shelf Res doi:10.1016/j.csr.2010.04.008 (in press)

Vermaat JE, McQuatters-Gollop A, Eleveld MA, Gilbert A (2008) Past, present and future nutrient loads of the North Sea: Causes and consequences. Estuar Coast Shelf Sci **80**(1):53-59. doi:10.1016/j.ecss.2008.07.005

Vos RJ, Ten Brummelhuis PJG, Gerritsen H (2000) Integrated data-modelling approach for suspended sediment transport on a regional scale. Coast Eng **41**:177-200. doi:10.1016/S0378-3839(00)00032-6

Wei J, Malanotte-Rizzoli P (2009) Validation and application of an ensemble Kalman filter in the Selat Pauh of Singapore. Ocean Dyn **60**:395-401. doi:10.1007/s10236-009-0253-y

Weston K, Fernand L, Nicholls J, Marca-Bell A, Mills D, Sivyer D, Trimmer M (2008) Sedimentary and water column processes in the Oyster Ground: A potentially hypoxic region of the North Sea. Mar Environ Res **65**:235-249. doi 10.1016/j.marenvres.2007.11.002

Wild-Allen K, Lane A, Tett P (2002) Phytoplankton, sediment and optical observations in Netherlands coastal water in spring, J Sea Res **47**(3-4):303-315. doi:10.1016/S1385-1101(02)00121